



Free-electron interactions with photonic GKP states: Universal control and quantum error correction

Gefen Baranes ^{1,2,*}, Shiran Even-Haim,^{1,*} Ron Ruimy,^{1,*} Alexey Gorlach,¹ Raphael Dahan,¹
Asaf A. Diringer ³, Shay Hacoheh-Gourgy,³ and Ido Kaminer ^{1,†}

¹*Solid State Institute, Technion-Israel Institute of Technology, Haifa 32000, Israel*

²*Department of Physics, MIT-Harvard Center for Ultracold Atoms and Research Laboratory of Electronics,
Massachusetts Institute of Technology, Cambridge, Massachusetts 02139, USA*

and Department of Physics, Harvard University, Cambridge, Massachusetts 02138, USA

³*Faculty of Physics, Technion-Israel Institute of Technology, Haifa 32000, Israel*



(Received 24 January 2023; accepted 23 October 2023; published 20 December 2023)

We show that the coherent interaction between free electrons and photons can be used for universal control of continuous-variable photonic quantum states in the form of Gottesman-Kitaev-Preskill (GKP) qubits. Specifically, we find that electron energy combs enable nondestructive measurements of the photonic state and can induce arbitrary gates. Moreover, a single electron interacting with multiple photonic modes can create highly entangled states such as Greenberger-Horne-Zeilinger states and cluster states of GKPs.

DOI: [10.1103/PhysRevResearch.5.043271](https://doi.org/10.1103/PhysRevResearch.5.043271)

I. INTRODUCTION

Quantum error correction is essential for reaching large-scale quantum computation. One prominent approach toward this goal is to encode qubit information on continuous variables [1,2] in quantum harmonic oscillators, known as bosonic codes. These codes, and most prominently the Gottesman-Kitaev-Preskill (GKP) code [1], facilitate quantum error correction for fault-tolerant quantum computation [3]. The generation and manipulation of GKP states is a formidable challenge, as it necessitates non-Gaussian operations that typically require strong nonlinearities.

Creating the required nonlinearity can rely on a wide range of physical mechanisms. The nonlinearity can arise from intrinsically nonquadratic Hamiltonians that can be realized in the optical regime using the Kerr effect [4,5] or postselection by number-resolving photonic measurements [6–8]. The GKP states can also be deterministically generated from cat states [9,10], which, however, still require nonlinearity for their generation. Such nonlinearities are typically counterproductive to the stabilization of GKP states since they increase decoherence by coupling to external degrees of freedom, even more so given that such states rely on a large average photon number.

Leading approaches for generating and manipulating GKP states rely on the coupling to matter ancilla qubits, which provide the necessary strong nonlinearity. Such a scheme was demonstrated experimentally with the vibrational motion

of trapped ions [11,12], with cavity photons at microwave frequencies coupled to superconducting qubits in circuit quantum electrodynamics (QED) [13]. A similar ancilla-based scheme was also recently suggested theoretically in optical frequencies using cavity QED [14].

Here we propose a different physical mechanism that provides the needed nonlinear interaction using free electrons that act as ancilla qubits. We show how the fundamental coherent interaction of free electrons and photons, perhaps the most basic interaction in QED, can provide the building blocks for universal quantum computing with GKP states. The interaction provides the strong nonlinearity needed for quantum error correction and universal control of GKP states. This interaction can be used in gate-based [15] and measurement-based [16] computational protocols.

A step in this direction has recently shown the free-electron-based generation of GKP states [17]. We now unveil the complete picture and show that the fundamental electron-photon interaction can be described as a conditional displacement (CD) gate when the free electron is shaped in the rotor GKP encoding [18]. The CD gate is the basic building block for universal computation and error correction with GKP states [13,19].

The idea to use free electrons in the context of quantum optics is inspired by recent advances in ultrafast electron microscopy. Specifically, our work relies on the inelastic scattering of free electrons by electromagnetic fields, which was famously observed in photon-induced near-field electron microscopy (PINEM) [20–27]. This nonlinear scattering provides the additional degrees of freedom required to encode quantum information on the individual electron by coherent modulation of its wave function [28–30]. The ability to control the modulated electrons has been studied extensively in theory (e.g., [31,32]) and experiments (e.g., [33–35]). The interaction of such modulated electrons enables photon addition and subtraction [36], measurement of light statistics [37], coherent

*These authors contributed equally to this work.

†kaminer@technion.ac.il

control of two-level systems [38–43], and investigation of ultrafast population dynamics of superradiance [44]. The same underlying theory enables heralded generation of photonic entanglement [45] and heralded generation of Fock states of one or more photons [46–49]. Such ideas and experimental achievements support the feasibility of the scheme we propose here.

The use of free electrons as matter ancilla qubits is intriguing for a few practical reasons. In contrast to currently used matter ancilla qubits, free electrons are versatile in their energy spectrum and can access a large range of frequencies, including the optical (and potentially higher) range. This versatility enables the transfer to the optical regime of concepts that were only demonstrated in the microwave regime, such as nonlinear ancilla qubits—potentially bypassing inherent technical limitations of scalability and low-temperature operation.

Moreover, the free electrons are fundamentally different from previously purposed matter ancilla qubits because they are *flying qubits*, meaning they only couple temporarily to the photonic mode before they continue propagating. The limited interaction time reduces the decoherence of the photonic mode by its coupling to the ancilla. This coupling decoherence can be characterized by multiple noisy channels, such as inverse-Purcell decay [50] and self-Kerr nonlinearities [51], which pose a stronger limitation for GKP states due to their larger photon number. These decoherence channels are reduced by the short interaction time of the flying electron qubit.

Another advantage provided by the electrons being flying qubits is that they naturally facilitate coupling between spatially separated photonic modes. Being flying qubits, such electron qubits enable the generation of multipartite highly entangled states such as Greenberger-Horne-Zeilinger (GHZ) states [52] and cluster states [16], important resources for quantum computation and communication [53–55]. Moreover, our approach is applicable not only for traveling GKP states, as the ones integrated on waveguides, but also for stationary GKP states in cavity modes. Any operation between such stationary cavity modes requires an interaction with a flying qubit, which is what the electron-photon interaction provides. These possibilities are presented in our work below, presenting specific schemes for GKP stabilization and for universal control. This aspect allows one not only to adopt concepts and protocols from the circuit QED and trapped ions communities, but also to create new protocols involving multimode interactions unique to free-electron-based systems.

II. FREE ELECTRONS AS ANCILLAS FOR CONDITIONAL DISPLACEMENT ON PHOTONIC STATES

We define the electron coherent energy comb as a superposition of electron energy states with a Gaussian envelope around a central energy E_0 ,

$$|\text{comb}_\sigma^\omega\rangle \propto \sum_n e^{-\frac{n^2}{2\sigma^2}} |E_0 + n\hbar\omega\rangle. \quad (1)$$

Here $|E_0\rangle$ is the state of an electron with mean energy E_0 and narrow energy distribution compared to $\hbar\omega$, ω is the

modulating laser frequency, and σ is the dimensionless energy width describing the number of energy states in the electron comb. This electron comb can be created by shaping a monoenergetic electron using multiple laser harmonics [31] or multiple interaction stages [32]. We note that an additional linear phase term $e^{in(\omega t - \phi)}$ with a global phase shift ϕ is omitted since it only describes a shift of the comb in time. This phase is directly controlled by the subcycle delay of the laser excitation, which is tuned between different stages in the system, such as between the electron modulation and the gate interactions. In this paper, we consider the limit of $\sigma \gg 1$, and omit the σ in the electron comb notation. In this case, the electron comb becomes an approximate eigenstate of the energy displacement operators $b_\omega, b_\omega^\dagger$ (satisfying $b_\omega b_\omega^\dagger = b_\omega^\dagger b_\omega = 1$). These operators describe a translation of $\hbar\omega$ in the electron’s energy, which corresponds to the photon ladder operators $a_\omega^\dagger, a_\omega$, describing emission or absorption of a single photon in a frequency ω , respectively.

The electron comb can be described as a qubit, encoded in the rotor GKP encoding [18], with the following basis:

$$\begin{aligned} |0\rangle_e &= \sum_n |E_0 + 2n\hbar\omega\rangle = |\text{comb}^{2\omega}\rangle, \\ |1\rangle_e &= \sum_n |E_0 + (2n + 1)\hbar\omega\rangle = b_\omega |\text{comb}^{2\omega}\rangle. \end{aligned} \quad (2)$$

We denote $|\psi\rangle_e = \alpha|0\rangle_e + \beta|1\rangle_e$ as a general free-electron qubit state. The $|0\rangle_e$ state can be generated via a typical electron comb generation scheme [31,32] using a modulation laser with frequency 2ω . Universal single-qubit gates [28] over such free-electron qubit states are achievable by multiple PINEM interactions separated by free-space propagation, i.e., drift. Free-space propagation over an appropriate distance corresponds to a rotation around the Z axis on the Bloch sphere, and PINEM interaction corresponds to a rotation around the X axis on the Bloch sphere [28]. See Fig. 1(c) and Appendix A.5. Coming back to the analogy of coherent light, if we consider the energy translation operator b_ω , then the electron qubit states are eigenstates of b_ω^2 and satisfy $\langle i|_e b_\omega |i\rangle_e \approx 0$ with $i = 0, 1$, similar to ladder operators acting on optical cat states. This observation creates an analogy between the creation of GKP states [17] and cat breeding protocols [9].

To describe the interaction of such modulated electrons with quantum photonic states, we quantize the electromagnetic field, as was presented theoretically in [56,57] and was in part demonstrated experimentally in [37]. Since photonic modes have multiple frequency components, the interaction can be described using the following scattering matrix, as shown in [58]

$$S = \exp \left[\int d\omega (g_{Q,\omega} b_\omega a_\omega^\dagger - g_{Q,\omega}^* b_\omega^\dagger a_\omega) \right]. \quad (3)$$

We define the electron-photon coupling strength $g_{Q,\omega}$ at a given frequency ω as in [59]. The coupling strength for a mode family is $|g_{Q,m}|^2 = \int d\omega |g_{Q,\omega}|^2$. The annihilation and creation operators of the mode family a_m and a_m^\dagger are found by integrating over all frequencies, $a_m = \frac{1}{g_{Q,m}} \int d\omega g_{Q,\omega}^* a_\omega$ and $a_m^\dagger = \frac{1}{g_{Q,m}} \int d\omega g_{Q,\omega} a_\omega^\dagger$. For the free-electron qubit, $b_\omega = b_\omega^\dagger = \sigma_x$ [see Fig. 1(b)]. We consider the case where the

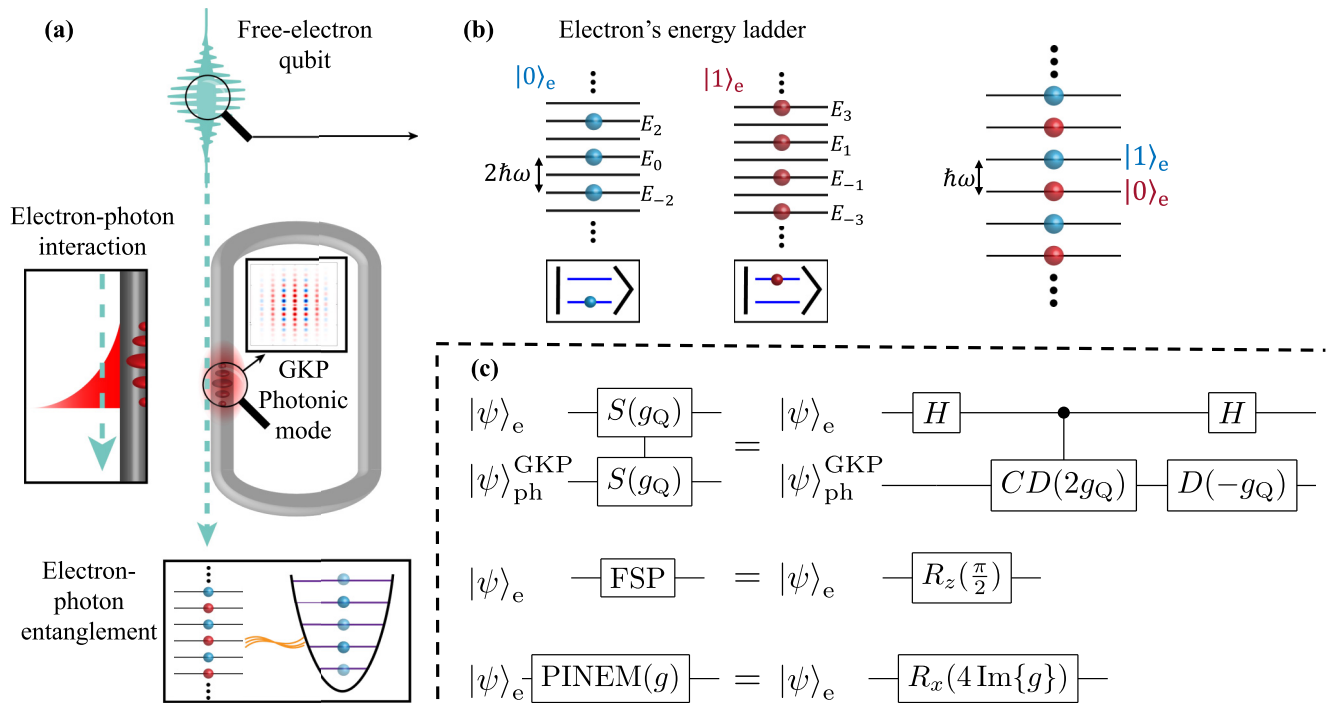


FIG. 1. The free-electron-photon interaction as a fundamental building block for quantum information processing. (a) The free electron is reshaped into a free-electron qubit state (e.g., using laser interactions [31,32]), which interacts with the photonic mode through a near-field coupling. The photonic mode contains a GKP state. The interaction entangles the electron with the GKP state. (b) The free-electron qubit states are shown by their energy spectra, as the even (blue, qubit $|0\rangle_e$) and odd (red, qubit $|1\rangle_e$) comb electrons with $2\hbar\omega$ energy spacing. (c) Building blocks for universal quantum computation on the free-electron qubit [28] and the GKP state (left) and their corresponding circuits (right). The first is the interaction scattering matrix, the second is the free-space propagation (FSP) operation on the electron, and the last is the PINEM operation on the electron describing interaction with classical coherent light.

coupling is with the multifrequency photonic mode, omitting the m in the notation. The scattering matrix in Eq. (3) is then reduced to a conditional displacement (CD) operator, controlled in the X basis:

$$\begin{aligned}
 S(g_Q) &= \exp(g_Q \sigma_x a^\dagger - g_Q^* \sigma_x a) = D(g_Q \sigma_x) \\
 &= |+\rangle_e \langle +|_e \otimes D(g_Q) + |-\rangle_e \langle -|_e \otimes D(-g_Q) \\
 &= \text{CD}(g_Q).
 \end{aligned} \tag{4}$$

$D(\alpha) = \exp(\alpha a^\dagger - \alpha^* a)$ is a coherent displacement operator [60]. g_Q is the coupling strength for a mode family, describing the interaction strength and the relative phase between the mode family and the free electron shaped by the modulating laser. The amplitude $|g_Q|$ is controlled by the overlap of the electron trajectory with the spatial shape of the mode, tunable by the distance of the electron beam from the evanescent part of the photonic mode [49]. The phase $\angle g_Q$ is tunable by a subcycle delay of the shaping laser that creates the free-electron qubit. All the photonic modes and modulating lasers are phase locked, as further elaborated upon in [17].

There is an intrinsic trade-off between the strength of interaction, which necessitates prolonged interaction, and the accuracy of the CD operator, which is reduced with the interaction length due to the dispersion, as detailed in [17]. Appendix F also qualitatively discusses the higher-order dispersion effects on the electron's fidelity. This effect imposes a limitation on the width of the comb electron.

The following sections show how the free-electron qubit can be used as an ancilla qubit in manipulating GKP states in a wide range of frequencies, including the optical range.

III. UNIVERSAL SINGLE-QUBIT GATES WITH FREE-ELECTRON ANCILLAS

For the universality section we focus on the case where the photonic mode is an ideal GKP state [1]. GKP states form a lattice in their Wigner representation [61] and can be defined by the lattice constants $a_{x,y,z}$ (see Appendix B). Pauli gates on the GKP qubit can be achieved in two ways. The first is using the CD operator from Eq. (4) and setting the coupling constant between the free electron and the photonic mode to be $g_Q = \pm \frac{a_i}{2}$, for $i = x, y, z$. The second is by deterministically displacing the photonic mode using a coherent light source coupled to the photonic modes containing the GKP state. The Hadamard (H) gate acts as a rotation in phase space. Therefore, it can be replaced by adding a $\pi/2$ phase to g_Q for all the following computation steps [62]. This phase can be added by a delay to the phase of the modulating laser for all the following electrons. These choices are analogous to the case of regular CD operations based on qubit ancillas [13,62].

When $g_Q = a_i/4$, Eq. (4) gives a controlled Pauli gate σ_i on the GKP state, controlled by the electron's state in the X basis. For a nonideal GKP state, the added displacement $D(-a_i/4)$ needs to be corrected (in postprocessing), to recenter the

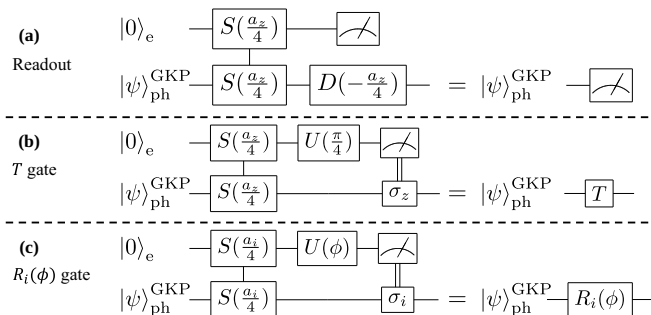


FIG. 2. Single-qubit gates induced by the free-electron ancilla. (a) Readout operation: using electron ancilla qubit with interaction $g_Q = \frac{a_z}{4}$, followed by a measurement of the electron to extract the GKP state. Using different axes can be used for readout with any Pauli operator. (b) Rotation gate $R_i(\phi)$ in the $i = x, y, z$ direction: using free-electron ancilla with $g_Q = \frac{a_i}{2}$ performs the gate controlled Pauli ($C\sigma_i$) on the GKP state, with the electron being the control qubit. Then the electron is measured in the basis $|\phi_{\pm}\rangle = \frac{1}{\sqrt{2}}(e^{i\phi/2}|0\rangle_e \pm e^{-i\phi/2}|1\rangle_e)$, using the unitary $U(\phi)$. For feedforward, if the measurement result is $|\phi_{-}\rangle$, the Pauli σ_i gate is applied. (c) T gate: example of rotation gate with $\phi = \frac{\pi}{4}$ and $i = z$.

code space. As an example, the CNOT gate between the free electron and the GKP state is given by $g_Q = a_x/4$:

$$\text{CNOT}_{e \rightarrow \text{ph}} = [H_e \otimes D(-a_x/4)]S(a_x/4)(H_e \otimes I). \quad (5)$$

Controlled Pauli gates give the ability to create maximum entanglement between the electron qubit and the GKP state. Moreover, controlled Pauli gates can be used to read out the GKP state by measuring the electron’s energy as an ancilla [15] [Fig. 2(a)].

The CD operator and rotation gates on the ancilla qubit can be used to implement a universal set of gates on the GKP state with an additional feedforward mechanism. In the feedforward mechanism, the next operation is done according to the electron’s measurement result. Further discussion of the feedforward mechanism is in Sec. IV. Rotation gates around $i = x, y, z$ axis with angle ϕ , $R_i(\phi)$, are achieved with teleported gates by an ancilla qubit [62,63], as shown in Fig. 2(c). The initial state of the electron is $|0\rangle_e$. The electron interacts with the GKP state with $g_Q = \frac{a_i}{4}$, $i = x, y, z$ according to the rotation axis and is then measured in the $|\phi_{\pm}\rangle_e = 1/\sqrt{2}(e^{i\phi/2}|0\rangle_e \pm e^{-i\phi/2}|1\rangle_e)$ basis. The ability to coherently control the electron’s qubit state [28] allows measuring it

in any desired basis, with additional drift and PINEM interactions for the postinteraction electron. If the measurement result is $|\phi_{-}\rangle_e$, the Pauli gate σ_i is applied to the GKP state, and if the measurement result is $|\phi_{+}\rangle_e$ there is no need to apply any gate. See Appendix C 5 for details on measuring in the $|\phi_{\pm}\rangle_e$ basis. The S and T gates can be achieved by rotations around the Z axis, with the angles $\frac{\pi}{2}$ and $\frac{\pi}{4}$, respectively.

The gates requiring feedforward, rotation $R_i(\phi)$, and $\text{CNOT}_{\text{ph}1 \rightarrow \text{ph}2}$, as shown in Table I, are based on teleported gates [62,63]. Depending on the measurement outcome, an additional Pauli operation may need to be implemented. In a quantum circuit application, these feedforward Pauli operations can be commuted to the end of the quantum circuit in a procedure known as modifying the Pauli frame [16]. Using the Pauli frame allows avoiding the application of Pauli gates in teleported gates [64].

Altogether, the free-electron qubit ancilla is a universal tool for quantum computation with GKP states in a photonic mode. The fundamental free-electron-photon interaction is the computational mechanism, that can be implemented and controlled in ultrafast electron microscopes [20,23,32,34,37,65].

IV. FREE-ELECTRON INTERACTION AS A STABILIZER AND ERROR CORRECTION TOOL

This section describes the stabilization and error correction process with the free electron. General error correction involves measurements of the stabilizers and correcting accordingly. The CD operator from Eq. (4) can stabilize the GKP manifold. Some schemes for GKP manifold stabilization [13,66] use multiple consecutive CD interactions, performing the error correction without feedforward of the measurement result. On the contrary, the free-electron ancilla can interact only once with the photonic mode before propagating, necessitating a feedforward mechanism as in other more conventional approaches [67]. Measurement of the stabilizers is achieved by interaction with a coupling constant equal to the lattice constant, $g_Q = \pm a_i$, followed by a measurement of the free electron. Combining the free-electron-photon interaction and feedforward mechanism allows for error correction and stabilization of the GKP manifold. Furthermore, applying a single round of stabilizer measurement and correction improves the fidelity of the photonic mode state compared to a desired GKP state for any initial state.

With current experimental abilities, it is feasible to apply a single round of stabilizer measurement and correction with

TABLE I. Operations on the photonic state created by a free-electron ancilla for universal quantum computation. Row 1 describes the coupling constant and electron state needed for creating Pauli gates σ_i on the GKP state. Row 2 describes how to use the electron qubit for the readout of the GKP state. Row 3 is the rotation gate R_i by angle ϕ , created using a teleported gate with feedforward. Row 4 shows how to use two electron qubits to create a CNOT gate between two GKP states in different photonic modes.

Operation	g_Q	Electron state	Feedforward
Pauli gates σ_i	$a_i/2$	$ +\rangle_e$	No
Readout in i basis	$a_i/4$	$ 0\rangle_e$	No
Rotation $R_i(\phi)$	$a_i/4$	$ 0\rangle_e$	If $ \phi_{+}\rangle_e$ is measured—none If $ \phi_{-}\rangle_e$ is measured— σ_i gate
$\text{CNOT}_{\text{ph}1 \rightarrow \text{ph}2}$	$g_{Q,1} = \frac{a_z}{4}, g_{Q,2} = \frac{a_x}{4}$	$ 0\rangle_e$	If $ 0\rangle_e$ is measured—none If $ 1\rangle_e$ is measured— σ_z gate

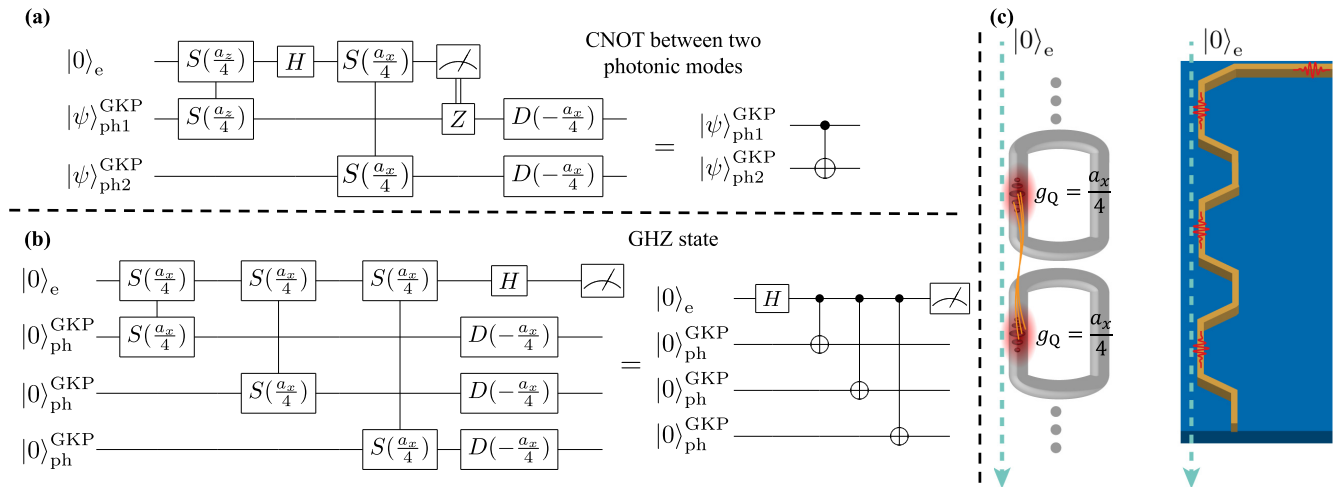


FIG. 3. Creation of multiqubit entanglement using free electrons. (a) $CNOT_{ph1 \rightarrow ph2}$ gate between two GKP states. (b) The scheme for generating a GHZ state of three GKP states. (c) Two approaches for implementing the GHZ state: stationary GKP states in cavities (left) and propagating GKP states in a waveguide (right).

feedforward (see discussion for further information). Since error correction protocols stabilize the GKP manifold, arbitrary states can become closer to GKP states. This fact can be used to increase the success probability of probabilistic GKP generation mechanisms. For example, our previous work [17] proposed a probabilistic optical GKP generation from squeezed vacuum using free-electron interaction, with a 31.25% success probability. Combining a single feedforward round in such probabilistic schemes increases the final state fidelities and probability of success for GKP generation. The details for these corrections are described in Appendix E.

V. FREE ELECTRON AS A FLYING QUBIT: CREATION OF GHZ AND CLUSTER STATES

The unique property of a free-electron ancilla as a flying qubit is that a single electron can be used for entangling multiple GKP states. The protocol for a $CNOT_{ph1 \rightarrow ph2}$ gate between two GKP states in two separated photonic modes is described in Fig. 3(a), where one electron qubit interacts with two GKP states. The electron starts in the state $|0\rangle_e$ and interacts with the first GKP state with $g_Q = \frac{a_x}{4}$, then changes the basis using a Hadamard gate (H_e) on the electron (see Appendix D 1), and then interacts with the second GKP state with $g_Q = \frac{a_x}{4}$. The last step of the protocol for $CNOT_{ph1 \rightarrow ph2}$ uses feedforward: the electron is measured, and if the measurement result is $|0\rangle_e$, then nothing is applied, but if the measurement result is $|1\rangle_e$, then a Pauli σ_z gate is applied to one of the GKP states. The $CNOT_{ph1 \rightarrow ph2}$ and the universal set of one qubit gates shown in the previous section are sufficient for universal quantum computing [15].

The maximally entangled GHZ state can be produced using one electron qubit interacting with multiple photonic GKP states. Each interaction is a $CNOT_{e \rightarrow ph}$, which can be implemented with $g_Q = a_x/4$, as presented in Eq. (5). In the final step of creating the GHZ state, the Hadamard gate is applied to the electron. The electron is then measured to disentangle it from the GKP states. Ultimately, a $D(-a_x/4)$ correction should be applied by using one $|+\rangle_e$ electron with $g_Q = -\frac{a_x}{4}$

interacting with all the GKP states to displace it back to the center of the phase space. The procedure is shown in Fig. 3(b).

This scheme of GHZ state creation can be realized using photonic cavities or waveguides, as shown in Fig. 3(c). The GKP states must be all phase matched to the electron; i.e., the phase velocity of each mode must be equal to the velocity of the electron wave function [34]. Such phase matching conditions were satisfied in experiments over distances of up to 500 μm [34], and have been achieved in several distinct configurations since [35,37,49,68]. For the cavities approach, all cavities need to be locked, i.e., with the same spectrum up to the coherent width of the electron. For the waveguide approach, the path between the interaction points must match the electron's path such that the electron will overlap with the GKP states in time. For example, this requirement can be satisfied by designing the repetition time of the GKP pulses plus the time it takes for the electron to go between the interaction points to be equal to the time it takes for the GKP mode to go between the two interaction points.

The prospects of free-electron flying qubits include the potential to create the cluster states needed for measurement-based quantum computation schemes. In recent years, much effort has been invested in measurement-based photonic quantum computation, specifically in the optical range. Such schemes require the efficient generation of photonic states and their entanglement into cluster states [16]. Clusters of GKP states [69] are especially desirable because GKP states are robust against photon loss errors [1], and can be easily measured in a different basis with the same operation, as shown in Fig. 2.

Following [70], we can add appropriate propagation distances between the subsequent interactions in the GHZ-creation scheme (shown in the previous section) to add single-qubit rotation on the electron and create a one-dimensional (1D) cluster of GKP states using a single electron [Fig. 4(a)]. Additionally, combining multiple electron channels can create two-dimensional (2D) and potentially higher-dimensional cluster states, as shown in Fig. 4(b). These higher-dimensional schemes are based on the protocol

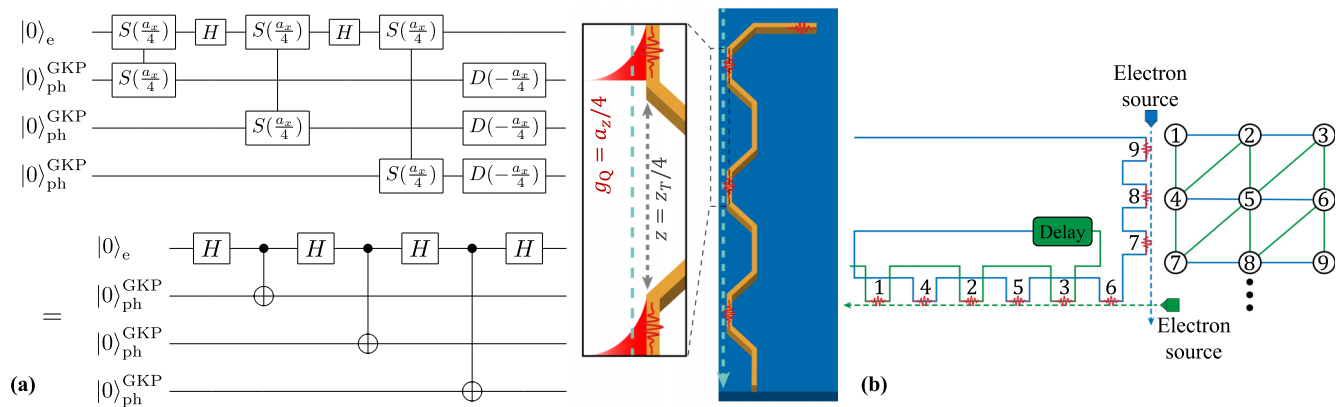


FIG. 4. Using flying qubits for the generation of cluster states. (a) A scheme for generating a 1D cluster state of GKP states in a photonic waveguide. Quantum circuit description of the proposed scheme (left) and a possible physical scheme using propagating GKP states in a waveguide (right). (b) Generation of 2D cluster states of GKP states. A possible implementation using a waveguide, two free-electron sources, and a delay (left). Visualization of the resulting 2D cluster state (right).

presented in [71] (further discussed in Appendix D 2 B). Consequently, free-electron interactions can be used as a building block in measurement-based photonic quantum computation schemes.

VI. DISCUSSION AND OUTLOOK

In summary, this paper demonstrates how the coherent interaction between free electrons and GKP states enables projective measurements, error correction, and universal control over the GKP states. This paper also demonstrates how the interaction of multiple GKP states with the same electron enables the creation of highly entangled states such as GHZ and cluster states. The key to these possibilities is the creation of CD based on the electron interaction. The electron-photon interaction thus reproduces other protocols for GKP state generation in superconducting qubits [13] and ion traps [12]. Going beyond these demonstrations, the free-electron implementation provides additional degrees of freedom to the interaction due to the intrinsic nature of the free electron as a flying qubit.

The use of free electrons as matter ancilla qubits is intriguing for a few practical reasons. In contrast to currently used matter ancilla qubits in circuit QED, trapped ions, and cavity QED counterparts [11–14], free electrons are versatile in their energy spectrum and can access a large range of frequencies. Second, the most significant difference is that the free-electron ancilla is a flying qubit. While photons also act as flying qubits, they do not exhibit the strong interactions usually needed to realize the operations required from ancilla qubits, such as CD. A flying ancilla qubit allows for high connectivity between the electron and multiple *spatially separated* photonic modes. This fact can enable possibilities that are hard to create in other systems, such as the generation of highly entangled GHZ and cluster states with only one ancilla electron (rather than multiple ancilla qubits [72,73] or multimode coupling [74], which further limits the coherence times and exponentially complicates the physical realization. The flying qubit nature of the electron also implies that it interacts with the GKP state only for a short time (typically single-picosecond timescales [34,37]). In “aloof”/grazing an-

gle experiments [75,76], electrons fly by tens of nanometers from the surface to minimize radiation damage. From this distance, the electrons can only excite lower-energy excitations and do not typically cause damage to the sample. Therefore, the coherence time of the photonic qubit is not significantly reduced by the free-electron interaction (unlike the case of interaction with ancilla qubits in circuit QED [77]).

It is also interesting to compare the interaction of free-electron qubits with GKP states to other schemes that can be realized in the optical range, such as the beam-splitter interaction of optical cat states [10,17]. Beam splitters can generate GKP states with low success probability using postselection. They can also enable entangling photonic states and creating cluster states for fault-tolerant measurement-based quantum computation. The free electron enables this, but can also apply additional operations, such as efficient GKP generation [17], operation, stabilization, and gate-based universal quantum computation. Another aspect that makes free-electron-based schemes promising arises from developments in fast electron counting detectors (especially direct detection schemes) [78]. Since free electrons are energetic particles, it is easier to achieve number-resolved electron detection than similar detection with photons.

As presented in this work, the electrons can stabilize the quantum state by performing error correction. The importance of GKP stabilization and error correction was demonstrated in microwave cavities [13,79]. The electron flying qubit can perform gates on such stationary modes in a manner that photonic flying qubits can only apply on traveling modes. Currently, to the best of our knowledge, there is no way to generate, stabilize, or manipulate GKP states while performing error correction inside optical cavities. Such abilities, if achieved, can open up new opportunities in quantum technologies, such as optical quantum memories [80], full-on error-correction gate-based quantum computation using stored GKP states at room temperature, or the integration of GKP states into other optical quantum computational systems such as optical cavity QED.

Since current electron sources are not deterministic, heralding the application of the gates or using feedforward is necessary. Recent experiments have shown opportunities for both photon-heralded electron sources by time-resolved

detection [47,48] and electron-heralded electron sources by antibunching [81,82]. Such heralding abilities, together with multiplexing, can be used for deterministic single-electron sources, similar to the current common approach for continuous-variable (CV) optical quantum computation [69,83].

Realizing free-electron-driven optical GKP states requires addressing crucial challenges in each of the two main stages of the process: initial electron qubit preparation and efficient electron-photon quantum interaction. Both stages are currently extensively investigated theoretically and experimentally.

For the first, free-electron qubits and single-qubit operations of limited fidelity are already generated in PINEM experiments [34,35,84]. Some of these experiments realized free-electron combs even before the theory work showed how such combs implement qubits [28]. Methods for increasing the fidelities of such combs (and thus of the qubits) are being developed (e.g., [31,32]). Other relevant ways of encoding qubits on free electrons (not via combs) were also demonstrated, as in [29], where the Bloch-sphere algebra of the qubit was demonstrated.

For the second, efficient electron-photon quantum interaction is now at the frontier of research and is advancing quickly (e.g., [58]). The realization of integrated photonic structures inside ultrafast electron microscopes contributed to these efforts [35,47]. The necessary coupling strengths have been recently realized using plasmonic structures [49] and photonic flatbands [85]. Our recent work [17] summarized these advances and drew a roadmap toward free-electron quantum information processing with continuous variables.

The electron detectors' response time limits the number of feedforward operations possible before the photonic mode loses coherence. Electron detectors' response times can be very fast [comparable to Avalanche photodiodes (APDs)], on the order of hundreds of picoseconds [86]. However, electronic latency delays the feedforward process to the order of 10 ns (the electron detector and the photonic chip are separated by a meter-scale distance). In the optical range, most optical material-limited loss time for a cavity with high confinement is on the order of 10 ns [87]. The current parameters indicate that it is possible to do approximately one feedforward operation. As discussed in Sec. IV, a single feedforward's time is sufficient since, in a quantum circuit application, the Pauli operations applied in the feedforward process can be commuted to the end of the quantum circuit in a procedure known as modifying the Pauli frame [16,64,69]. This circuit modification enables the computation of circuits with many feedforward gates, applying the total correction at the end, utilizing the same electronic latency in parallel. It is also important to note that electron cameras and detection technologies are not optimized for feedforward operation, and with time, the numbers are expected to improve.

The free electron can also be shaped to multilevel qudits with the GKP rotor encoding. By changing the electron comb energy gap from $2\hbar\omega$ to $N\hbar\omega$ [17,30], the free electron encodes an N -level qudit in the rotor encoding [18]. One can compare the rotor states to Pegg-Barnett phase states [88]; like the rotor states, they are not normalizable, but their approximation can still be used. Based on this analogy, the

approximated free-electron normalized states compare to the bosonic rotation codes state of qudit binomial or N -legged cat state. These states approximate the not-normalizable Pegg-Barnett phase states and can also be used to encode qudits by changing the spacings [89]. The binomial qudit code state and N -legged cat state can provide additional degrees of freedom that can be exploited for generating and controlling GKP states. However, they are extremely difficult to generate in optics. Free electrons can substitute these useful states and provide additional degrees of freedom. This research direction facilitates the tunability of free electrons to provide degrees of freedom that fundamentally differ from their circuit QED or trapped-ion counterparts.

ACKNOWLEDGMENTS

We thank Eyal Finkelshtein for the valuable conversations and insights. This research is funded in part by the Gordon and Betty Moore Foundation, through Grant No. GBMF11473. The research was also supported by the European Research Council (ERC Starting Grant No. 851780-NanoEP), the European Union Horizon 2020 Research and Innovation Program (under Grant Agreement No. 964591 SMART-electron), the Israeli Science Foundation (ISF), Pazi Foundation, and Technion's Helen Diller Quantum Center. G.B. acknowledges the support of the Technion Excellence Program for undergraduate students and the MIT Physics Peskoff Fellowship for graduate students. S.E.-H. acknowledges the support of the Helen Diller Quantum Center Merit Fellowship. R.R. acknowledges the support of the Adams Fellowship of the Israeli Academy of Sciences and Humanities. R.D. acknowledges the support of the Council for Higher Education Support Program for Outstanding Ph.D. Candidates in Quantum Science and Technology in Research Universities.

APPENDIX A: FREE ELECTRONS AS QUDITS

This section focuses on the free electron's state. We will describe the electron as a qudit, showing the case of two-level and four-level systems.

1. Free electrons as two-level and four-level systems

Let us introduce an N -level comb electron, with an energy difference of $N\hbar\omega$, a shift in energy by $m\hbar\omega$, and a Gaussian envelope σ around a central energy E_0 :

$$|\text{comb}_{\sigma,\phi}^{m,N}\rangle_e \propto \sum_{n=-\infty}^{\infty} e^{-\frac{n^2}{2\sigma^2}} e^{i\phi n} |E_0 + \hbar\omega(Nn - m)\rangle. \quad (\text{A1})$$

To create an electron qubit, we consider a comb electron with an energy difference of $2\hbar\omega$. The $|0\rangle_e$ state is

$$|0\rangle_e = |\text{comb}_{\sigma,\phi=0}^{0,2}\rangle_e \propto \sum_{n=-\infty}^{\infty} e^{-\frac{n^2}{2\sigma^2}} |E_0 + \hbar\omega 2n\rangle. \quad (\text{A2})$$

The $|1\rangle_e$ state, orthogonal to the $|0\rangle_e$ state, is

$$|1\rangle_e = |\text{comb}_{\sigma,\phi=0}^{1,2}\rangle_e \propto \sum_{n=-\infty}^{\infty} e^{-\frac{n^2}{2\sigma^2}} |E_0 + \hbar\omega(2n - 1)\rangle. \quad (\text{A3})$$

The X basis will be built out of the general comb electron states as follows:

$$|+\rangle_e = |\text{comb}_{\sigma,\phi=0}^{0,1}\rangle_e, \quad |-\rangle_e = |\text{comb}_{\sigma,\phi=\pi}^{0,1}\rangle_e. \quad (\text{A4})$$

Using $N = 4$, the electron can act as a four-level system. The basis states are

$$\begin{aligned} |00\rangle_e &= |\text{comb}_{\sigma,\phi=0}^{0,4}\rangle_e, & |01\rangle_e &= |\text{comb}_{\sigma,\phi=0}^{1,4}\rangle_e, \\ |10\rangle_e &= |\text{comb}_{\sigma,\phi=0}^{2,4}\rangle_e, & |11\rangle_e &= |\text{comb}_{\sigma,\phi=0}^{3,4}\rangle_e. \end{aligned} \quad (\text{A5})$$

2. Interaction Hamiltonian as a conditional gate

The scattering matrix describes the interaction between the electron and the photonic modes, and was introduced in Eq. (3) in the main text. When the electron is in the electron qubit sub-Hilbert space, the operator b_ω becomes the Pauli operator σ_x [28]. Thus the scattering matrix alters into a displacement operator:

$$\begin{aligned} S(g_Q) &= D(\sigma_x g_Q) = e^{\sigma_x[\Re\{g_Q\} + i\Im\{g_Q\}]a^\dagger - [\Re\{g_Q\} - i\Im\{g_Q\}]a} \\ &= e^{\sigma_x[\Re\{g_Q\}(a^\dagger - a) + i\Im\{g_Q\}(a^\dagger + a)]}. \end{aligned} \quad (\text{A6})$$

We will use the connection between the annihilation and creation operators a, a^\dagger , and the position and momentum operators x, p :

$$a = \frac{1}{\sqrt{2}}(x + ip), \quad a^\dagger = \frac{1}{\sqrt{2}}(x - ip). \quad (\text{A7})$$

Thus

$$S(g_Q) = e^{i\sqrt{2}(-\Re\{g_Q\}p + \Im\{g_Q\}x)\sigma_x}. \quad (\text{A8})$$

Therefore, the scattering matrix can be written as a conditional displacement in the electron's X basis, as follows:

$$\begin{aligned} S(g_Q) &= D(g_Q \sigma_x) \\ &= |+\rangle_e \langle +|_e \otimes D(g_Q) + |-\rangle_e \langle -|_e \otimes D(-g_Q) \\ &= \frac{1}{2} \{ [D(g_Q) + D(-g_Q)]I + [D(g_Q) - D(-g_Q)]\sigma_x \} \\ &= CD(g_Q). \end{aligned} \quad (\text{A9})$$

3. Using electrons in the X basis

Using electrons in the X basis, $|+\rangle_e, |-\rangle_e$ will create a deterministic displacement gate on the photonic mode. Following Eq. (A9), acting with a $|+\rangle_e$ will create a $D(g_Q)$ gate, and acting with a $|-\rangle_e$ will create a $D(-g_Q)$ gate on the photonic mode. No entanglement is induced between the electron and the photonic mode, and the electron state is not changed in the interaction. Using this knowledge, one can use a regular comb electron to create any displacement gate on the photonic mode (up to a physical value of g_Q).

4. Using electrons in the Z basis

Using electrons in the Z basis, $|0\rangle_e, |1\rangle_e$ will create Kraus operators on the photonic mode, after postselection. Using Eq. (A9), the final joint state after an interaction of electron state $|0\rangle_e$ and a general photonic state $|\psi\rangle_{\text{ph}}$ is

$$\begin{aligned} |\psi\rangle_{\text{final}} &= S(g_Q)|0\rangle_e|\psi\rangle_{\text{ph}} \\ &= [|+\rangle_e \langle +|_e D(g_Q) + |-\rangle_e \langle -|_e D(-g_Q)]|0\rangle_e|\psi\rangle_{\text{ph}} \\ &= [|0\rangle_e M^+(g_Q) + |1\rangle_e M^-(g_Q)]|\psi\rangle_{\text{ph}}, \end{aligned} \quad (\text{A10})$$

while we defined the Kraus operators as

$$M^\pm(g_Q) = [D(g_Q) \pm D(-g_Q)]/2. \quad (\text{A11})$$

$M^+(g_Q)$ acts after measuring $|0\rangle_e$ and $M^-(g_Q)$ acts after measuring $|1\rangle_e$. For an initial $|1\rangle_e$ electron state, the final state is

$$|\psi\rangle_{\text{final}} = [|0\rangle_e M^-(g_Q) + |1\rangle_e M^+(g_Q)]|\psi\rangle_{\text{ph}}. \quad (\text{A12})$$

For an initial general electron state $|\phi\rangle_e = \cos\theta|0\rangle_e + e^{i\varphi}\sin\theta|1\rangle_e$, the final state is

$$\begin{aligned} |\psi\rangle_{\text{final}} &= S(g_Q)|\phi\rangle_e|\psi\rangle_{\text{ph}} \\ &= [(\cos\theta|0\rangle_e + e^{i\varphi}\sin\theta|1\rangle_e)M^+(g_Q) \\ &\quad + (e^{i\varphi}\sin\theta|0\rangle_e + \cos\theta|1\rangle_e)M^-(g_Q)]|\psi\rangle_{\text{ph}}. \end{aligned} \quad (\text{A13})$$

Using four-level comb electrons, one can operate in two orthogonal axes in phase simultaneously. After one interaction of $|00\rangle_e$ with a general photonic mode state, the final state is

$$\begin{aligned} |\psi\rangle_{\text{final}} &= S(g_Q)|00\rangle_e|\psi\rangle_{\text{ph}} \\ &= \frac{1}{4} \begin{bmatrix} |00\rangle_e (D_{g_Q} + D_{ig_Q} + D_{-g_Q} + D_{-ig_Q}) \\ + |01\rangle_e (D_{g_Q} + iD_{ig_Q} - D_{-g_Q} - iD_{-ig_Q}) \\ + |10\rangle_e (D_{g_Q} - D_{ig_Q} + D_{-g_Q} - D_{-ig_Q}) \\ + |11\rangle_e (D_{g_Q} - iD_{ig_Q} - D_{-g_Q} + iD_{-ig_Q}) \end{bmatrix} |\psi\rangle_{\text{ph}}. \end{aligned} \quad (\text{A14})$$

5. Universal control over the electron qubit

As shown in [28,29], free-electron qubits can be controlled universally with two components. The first is interaction with classical coherent light, classical PINEM, with interaction constant g :

$$\begin{aligned} \text{PINEM}(g) &= R_x(4\Im\{g\}) \\ &= \begin{pmatrix} \cos(2\Im\{g\}) & -i\sin(2\Im\{g\}) \\ -i\sin(2\Im\{g\}) & \cos(2\Im\{g\}) \end{pmatrix}, \end{aligned} \quad (\text{A15})$$

while $g = \frac{e}{\hbar\omega} \int_{-\infty}^z dz' E_z(z', x, y) e^{-\frac{i\omega}{v}z'}$ depends on the transverse directions x, y and the integration limit z in the direction parallel to the electron's momentum. E_z is the electric field in the z direction, ω is the shaping laser's phase, and v is the electron velocity.

The second is free-space propagation (FSP), applying $R_z(\pi/2)$. FSP changes each energy component of the electron, $U(\phi)|n\rangle_e = e^{-i\phi n^2}|n\rangle_e$. ϕ is defined by $2\pi \frac{z}{z_T}$ with z being the propagation distance, and $z_T = \frac{4\pi\gamma^3 m_e v^3}{\hbar} \omega^2$ is the Talbot distance [29]. m_e is the electron mass, v is its average velocity, and γ is the Lorentz factor. As the electron propagates, the phases accumulated take the electron out of the electron qubit sub-Hilbert space. However, propagation distance $z = \frac{z_T}{4}$ corresponds to a rotation gate on the electron's Bloch sphere of $\frac{\pi}{2}$ around the z axis [28]. Thus, when designing an experiment, the distance between the interactions of the electron with the photonic modes must be an integer multiple of this value. For simplicity, when we mark the FSP operation, we consider free propagation of $\frac{z_T}{4}$ such that $\text{FSP} = R_z(\pi/2)$. The following sequence can create the Hadamard (H) gate on the electron:

$$H_e = \text{FSP} \times \text{PINEM}(i\pi/8) \times \text{FSP}. \quad (\text{A16})$$

APPENDIX B: LIGHT AS A QUBIT

This section focuses on the photonic mode, describing it as a qubit in the continuous-variable approach. [17] Gottesman-Kitaev-Preskill (GKP) states appear to be the leading candidates for correcting errors when encoding qubits into oscillators. Our previous paper [17] described creating these states using the qubit comb electrons. This paper focuses on using free electrons for controlling the photonic modes, specifically GKP states. Thus we will elaborate on a few properties of the GKP state. There are two main types of GKP states—rectangular lattice and hexagonal lattice. Let us define the lattice constants for each option:

$$\begin{aligned} \text{square lattice: } & a_x = \alpha, \quad a_y = \alpha(1+i), \quad a_z = i\alpha, \\ \text{hexagonal lattice: } & a_x = \beta, \quad a_y = \beta e^{i\pi/3}, \quad a_z = \beta e^{i2\pi/3}, \end{aligned} \quad (\text{B1})$$

with $\alpha = \sqrt{2\pi}$ and $\beta = \sqrt{4\pi}/\sqrt{3}$. a_x and a_z are the distances between the lattice points in the two main lattice directions, connected to Pauli σ_x and σ_z , accordingly. For any GKP state, $\Im\{a_x a_y\} = 4\pi$. $a_y = a_x + a_z$ depends on the other two and is defined here to connect to Pauli σ_y .

APPENDIX C: SINGLE-QUBIT GATES ON THE PHOTONIC MODES

This section shows that free-electron qubits can be used for universal control over the photonic state. A set of universal quantum gates is any set of gates to which any operation possible on a quantum computer can be reduced.

1. Pauli gates and stabilizers

For an ideal GKP state, the stabilizers are

$$s_i = D(\pm a_i), \quad (\text{C1})$$

with $i = x, y, z$. One can use the following identities to displace the state in phase space:

$$D(c) = e^{-i\sqrt{2}c\hat{p}}, \quad D(ic) = e^{i\sqrt{2}c\hat{x}}, \quad (\text{C2})$$

where c is real, representing the displacement distance. Pauli gates can be found by the following formula:

$$\sigma_i = D\left(\pm \frac{a_i}{2}\right), \quad (\text{C3})$$

using $i = x, y, z$ once again. All these gates and stabilizers can be created using interactions with comb electrons $|+\rangle_e$ with the coupling $g_Q = \pm a_i$ for the stabilizers and $g_Q = \pm a_i/2$ for the Pauli gates ($i = x, y, z$).

2. Projections

The electron qubit to can be used to create projection operators on the photonic state. Using the free-electron qubit in the state $|0\rangle_e$, and choosing $g_Q = a_i/4$, $i = x, y, z$, the Kraus operators, defined in Eq. (A11), become projection operators:

$$\begin{aligned} M^\pm\left(\frac{a_i}{4}\right) &= D\left(\frac{a_i}{4}\right) \frac{1}{2} (I \pm \sigma_i) \\ &= D\left(\frac{a_i}{4}\right) |\pm i\rangle_{\text{ph}}^{\text{GKP}} \langle \pm i|_{\text{ph}}^{\text{GKP}} : -D\left(\frac{a_i}{4}\right) P_i^\pm, \end{aligned} \quad (\text{C4})$$

with the projections acting as follows:

$$\begin{aligned} P_i^\pm |\pm i\rangle_{\text{ph}}^{\text{GKP}} &= (|\pm i\rangle_{\text{ph}}^{\text{GKP}} \langle \pm i|_{\text{ph}}^{\text{GKP}}) |\pm i\rangle_{\text{ph}}^{\text{GKP}} = |\pm i\rangle_{\text{ph}}^{\text{GKP}}, \\ P_i^\pm |\mp i\rangle_{\text{ph}}^{\text{GKP}} &= (|\pm i\rangle_{\text{ph}}^{\text{GKP}} \langle \pm i|_{\text{ph}}^{\text{GKP}}) |\mp i\rangle_{\text{ph}}^{\text{GKP}} = 0. \end{aligned} \quad (\text{C5})$$

We defined $|\pm i\rangle_{\text{ph}}^{\text{GKP}}$ as the eigenvalue of σ_i for $i = x, y, z$.

3. Readout

Let us show how to measure in the X direction. Start with a general GKP state in the X basis, $|\psi_i\rangle_{\text{ph}} = \alpha|+\rangle_{\text{ph}}^{\text{GKP}} + \beta|-\rangle_{\text{ph}}^{\text{GKP}}$. The initial electron state is $|0\rangle_e$. In that case, according to Eq. (A10), the final state after the interaction is

$$|\psi_f\rangle = [|0\rangle_e M^+(g_Q) + |1\rangle_e M^-(g_Q)] (\alpha|+\rangle_{\text{ph}}^{\text{GKP}} + \beta|-\rangle_{\text{ph}}^{\text{GKP}}). \quad (\text{C6})$$

Here we will use the projection operators, by choosing $g_Q = a_x/4$. Thus the final state can be written as

$$|\psi_f\rangle = D(a_x/4) (\alpha|0\rangle_e |+\rangle_{\text{ph}}^{\text{GKP}} + \beta|1\rangle_e |-\rangle_{\text{ph}}^{\text{GKP}}). \quad (\text{C7})$$

Measuring the quantum state of the electron qubit is equivalent to measuring the GKP state in the X basis. Note that a displacement of $D(-a_x/4)$ is necessary to return the final photonic mode state into a GKP state, by deterministically using an electron $|+\rangle_e$ with $g_Q = -\frac{a_x}{2}$. To change this scheme and measure in the Y or Z basis, all that is needed is to change $a_x \rightarrow a_y, a_z$ accordingly.

4. Hadamard gate on the photonic mode

The Hadamard (H) gate on the GKP state is a rotation in phase space [62]. This gate can be achieved digitally by adding a $\pi/2$ phase shift to the calculated g_Q in the requested computation step and all the following steps.

Another option is to use a four-level comb electron, specifically choosing the initial state $|00\rangle_e$ and choosing $g_Q = a_x/2$. According to Eq. (A14), when starting from a general GKP state in the Z basis, $|\psi_i\rangle_{\text{ph}} = \alpha|0\rangle_{\text{ph}}^{\text{GKP}} + \beta|1\rangle_{\text{ph}}^{\text{GKP}}$, the final state after the interaction is

$$\begin{aligned} |\psi_f\rangle &= S\left(\frac{a_x}{2}\right) |00\rangle_e (\alpha|0\rangle_{\text{ph}}^{\text{GKP}} + \beta|1\rangle_{\text{ph}}^{\text{GKP}}) \\ &= \frac{1}{2\sqrt{2}} [|00\rangle_e (\alpha|+\rangle_{\text{ph}}^{\text{GKP}} + \beta|-\rangle_{\text{ph}}^{\text{GKP}}) \\ &\quad + |10\rangle_e (\beta|+\rangle_{\text{ph}}^{\text{GKP}} - \alpha|-\rangle_{\text{ph}}^{\text{GKP}})]. \end{aligned} \quad (\text{C8})$$

If we measure $|00\rangle_e$, we have success. Otherwise, a σ_y gate on the GKP is required, the $|+\rangle_e$ comb electron with $g_Q = a_y$. For the completeness of this section, let us show how the gate acts on the GKP in the X basis, translating it to the Z basis:

$$\begin{aligned} |\psi_f\rangle S\left(\frac{a_x}{2}\right) |00\rangle_e (\alpha|+\rangle_{\text{ph}}^{\text{GKP}} + \beta|-\rangle_{\text{ph}}^{\text{GKP}}) &= \\ = \frac{1}{2\sqrt{2}} [|00\rangle_e (\alpha|0\rangle_{\text{ph}}^{\text{GKP}} + \beta|1\rangle_{\text{ph}}^{\text{GKP}}) \\ &\quad + |10\rangle_e (\alpha|1\rangle_{\text{ph}}^{\text{GKP}} - \beta|0\rangle_{\text{ph}}^{\text{GKP}})]. \end{aligned} \quad (\text{C9})$$

From here we will use the same process. If we measure $|00\rangle_e$, we have success. Otherwise, we will use one $|+\rangle_e$ comb with $g_Q = a_y$ to create a σ_y gate on the GKP state.

5. Rotation gate

To get a rotation gate on the GKP state, an ancilla qubit can be used for teleported gates [11,13,62]. Using this scheme, the free-electron qubit is the ancilla qubit. One can apply a rotation gate around the X , Y , or Z axis at any angle ϕ , implemented with teleported gates, as shown in Fig. 2(b) in the main text.

We consider the case of a rotation of the GKP state $R_i(\phi)$, where $i = x, y, z$. We can write the state of the GKP state in the i basis as

$$|\psi\rangle_{\text{ph}}^{\text{GKP}} = \alpha|+\rangle_{\text{ph}}^{\text{GKP}} + \beta|-\rangle_{\text{ph}}^{\text{GKP}}. \quad (\text{C10})$$

The teleported gate protocol starts with preparing the electron in the state $|0\rangle_e$. We then apply a conditional displacement with $g_Q = \frac{a_i}{4}$, $i = x, y, z$. Finally, we use the unconditional displacement $D(g_Q)$ to recenter the code. At the end of the sequence, the joint final state is

$$\begin{aligned} |\psi\rangle_{\text{final}} &= \frac{\alpha}{2}(\mathbf{I} + \sigma_i)|0\rangle_e|+\rangle_{\text{ph}}^{\text{GKP}} + \frac{\alpha}{2}(\mathbf{I} - \sigma_i)|1\rangle_e|+\rangle_{\text{ph}}^{\text{GKP}} \\ &\quad + \frac{\beta}{2}(\mathbf{I} + \sigma_i)|0\rangle_e|-\rangle_{\text{ph}}^{\text{GKP}} + \frac{\beta}{2}(\mathbf{I} - \sigma_i)|1\rangle_e|-\rangle_{\text{ph}}^{\text{GKP}} \\ &= \alpha|0\rangle_e|+\rangle_{\text{ph}}^{\text{GKP}} + \beta|1\rangle_e|-\rangle_{\text{ph}}^{\text{GKP}}. \end{aligned} \quad (\text{C11})$$

We then measure the electron along an axis rotated by an angle ϕ from the X axis, in the $|\phi_{\pm}\rangle$ basis:

$$|\phi_{\pm}\rangle = \frac{1}{\sqrt{2}}(e^{\frac{i\phi}{2}}|0\rangle_e \pm e^{-\frac{i\phi}{2}}|1\rangle_e). \quad (\text{C12})$$

The Kraus operators acting on the GKP state, depending on the measurement outcome, are

$$K(\phi_{\pm}) = \frac{1}{\sqrt{2}}(e^{\frac{i\phi}{2}}|+\rangle\langle +|_{\text{ph}}^{\text{GKP}} \pm e^{-\frac{i\phi}{2}}|-\rangle\langle -|_{\text{ph}}^{\text{GKP}}). \quad (\text{C13})$$

Applying a feedforwarded σ_i gate if the electron is found in $|\phi_{-}\rangle_e$, we find that $K(\phi_{\pm}) = R_i(\phi)|\psi\rangle_{\text{ph}}^{\text{GKP}}$, and the whole sequence performs an unconditional rotation $R_i(\phi)$ of the GKP state around the $i = x, y, z$ axis by an angle of $-\phi$ with $R_i(\phi) = e^{\frac{i\phi}{2}}|+\rangle\langle +|_{\text{ph}}^{\text{GKP}} \pm e^{-\frac{i\phi}{2}}|-\rangle\langle -|_{\text{ph}}^{\text{GKP}}$. To apply the respected rotation on the electron, we can use the PINEM interaction and FSP mentioned in Appendix A 5. As shown in [28], using both PINEM and FSP interactions is a universal set of one qubit gate; therefore it is possible to get every unitary operation. In the teleported gates scheme, we need to measure

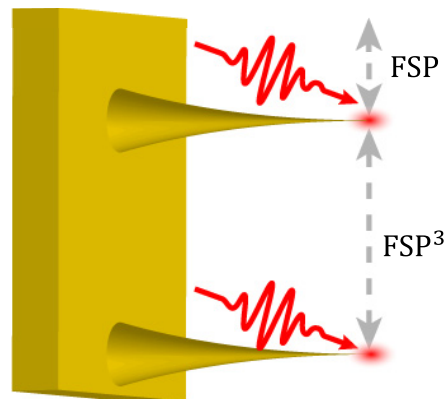


FIG. 5. Schematic of a device that implements a rotation gate on the free-electron qubit. This device implements the unitary operation $U(\phi)$, rotating the electron qubit from the computational basis to the $|\phi_{\pm}\rangle = \frac{1}{\sqrt{2}}(e^{\frac{i\phi}{2}}|0\rangle_e \pm e^{-\frac{i\phi}{2}}|1\rangle_e)$ basis. Performed by applying the following sequence: $U(\phi) = \text{PINEM}(4\Im\{g_2(\phi)\}) \times \text{FSP}^3 \times \text{PINEM}(4\Im\{g_1(\phi)\}) \times \text{FSP}$.

the electron in the basis of $|\phi_{\pm}\rangle = \frac{1}{\sqrt{2}}(e^{\frac{i\phi}{2}}|0\rangle_e \pm e^{-\frac{i\phi}{2}}|1\rangle_e)$. This can be achieved by applying on the electron, after the interaction with the photonic mode, a unitary operation to rotate the electron to the $|\phi_{\pm}\rangle$ basis.

To measure the electron in the $|\phi_{\pm}\rangle_e$ basis, a unitary $U(\phi)$ operation is applied on the electron before the measurement in the z basis, where $U(\phi)$ is defined as follows:

$$U(\phi) = \frac{1}{\sqrt{2}} \begin{pmatrix} e^{-\frac{i\phi}{2}} & e^{\frac{i\phi}{2}} \\ e^{-\frac{i\phi}{2}} & -e^{\frac{i\phi}{2}} \end{pmatrix},$$

$$U(\phi)|\phi_{+}\rangle_e = |0\rangle_e, \quad U(\phi)|\phi_{-}\rangle_e = |1\rangle_e. \quad (\text{C14})$$

Using the operations available for the free-electron qubit, FSP and PINEM, the unitary $U(\phi)$ is constructed by the following (see Fig. 5):

$$\begin{aligned} \text{PINEM}(g) &= R_x(4\Im\{g\}) = \begin{pmatrix} \cos(2\Im\{g\}) & -i \sin(2\Im\{g\}) \\ -i \sin(2\Im\{g\}) & \cos(2\Im\{g\}) \end{pmatrix}, \\ \text{FSP} &= \begin{pmatrix} 1 & 0 \\ 0 & i \end{pmatrix}, \\ U(\phi) &= \text{PINEM}(4\Im\{g_2(\phi)\}) \times \text{FSP}^3 \\ &\quad \times \text{PINEM}(4\Im\{g_1(\phi)\}) \times \text{FSP}. \end{aligned} \quad (\text{C15})$$

The unitary $U(\phi)$ is

$$\begin{aligned} U(\phi) &= \frac{1}{\sqrt{2}} \begin{pmatrix} e^{-\frac{i\phi}{2}} & e^{\frac{i\phi}{2}} \\ e^{-\frac{i\phi}{2}} & -e^{\frac{i\phi}{2}} \end{pmatrix} \\ &= \begin{pmatrix} \cos(a) \cos(b) + i \sin(a) \sin(b) & \cos(b) \sin(a) - i \cos(a) \sin(b) \\ -\cos(b) \sin(a) - i \cos(a) \sin(b) & \cos(a) \cos(b) - i \sin(a) \sin(b) \end{pmatrix}. \end{aligned} \quad (\text{C16})$$

When we mark the following values $a = 2\Im\{g_1(\phi)\}$, $b = 2\Im\{g_2(\phi)\}$, the solution is $g_1 = -i\pi/8$ and $g_2 = i(\pi + \phi)/4$. One could make a device that implements this unitary rotation

sequence. When there is no need to apply any $U(\phi)$, one could just not use any pulses in the two PINEM operations and get FSP^4 which is equal to the identity. The S and T gates can be

achieved by rotation around the z axis, with the angles $\frac{\pi}{2}$ and $\frac{\pi}{4}$, respectively.

APPENDIX D: MULTIQUBIT GATES AND ENTANGLEMENT

This section will elaborate on using free-electron qubits to create multiqubit gates between GKP states and to induce entanglement between multiple qubits.

1. Two-qubit gates: CNOT between photonic modes

In this section, we will present the full protocol for creating two-qubits gates between GKP states using free-electron qubits. The first photonic mode is in a general GKP state, $|\psi\rangle_{\text{ph1}}^{\text{GKP}} = \alpha|0\rangle_{\text{ph1}}^{\text{GKP}} + \beta|1\rangle_{\text{ph1}}^{\text{GKP}}$. The second photonic mode is in a general GKP state $|\psi\rangle_{\text{ph2}}^{\text{GKP}}$. The electron state is $|0\rangle_e$. For a CNOT gate the final state is expected to be

$$\begin{aligned} \text{CNOT}|\psi\rangle_{\text{ph1}}^{\text{GKP}}|\psi\rangle_{\text{ph2}}^{\text{GKP}} &= \text{CNOT}(\alpha|0\rangle_{\text{ph1}}^{\text{GKP}} + \beta|1\rangle_{\text{ph1}}^{\text{GKP}})|\psi\rangle_{\text{ph2}}^{\text{GKP}} \\ &= (\alpha|0\rangle_{\text{ph1}}^{\text{GKP}} + \beta|1\rangle_{\text{ph1}}^{\text{GKP}}\sigma_x)|\psi\rangle_{\text{ph2}}^{\text{GKP}}. \end{aligned} \quad (\text{D1})$$

According to the readout section, after the interaction of the electron with the first photonic mode, using $g_{Q1} = a_z/4$, the final state is

$$\begin{aligned} |\psi_{f,1}\rangle &= S^{(1)}\left(\frac{a_z}{4}\right)|0\rangle_e(\alpha|0\rangle_{\text{ph}}^{\text{GKP}} + \beta|1\rangle_{\text{ph}}^{\text{GKP}})|\psi\rangle_{\text{ph2}}^{\text{GKP}} \\ &= D^{(1)}\left(\frac{a_z}{4}\right)(\alpha|0\rangle_e|0\rangle_{\text{ph1}}^{\text{GKP}} + \beta|1\rangle_e|1\rangle_{\text{ph1}}^{\text{GKP}})|\psi\rangle_{\text{ph2}}^{\text{GKP}}, \end{aligned} \quad (\text{D2})$$

while $D^{(1)}(\frac{a_z}{4})$ is a displacement gate acting on the first mode. After the first interaction, we will induce a Hadamard gate on the electron qubit, H_e ; thus the final state will be

$$\begin{aligned} |\psi_{f,2}\rangle &= H_e|\psi_{f,1}\rangle \\ &= D^{(1)}\left(\frac{a_z}{4}\right)(\alpha|+\rangle_e|0\rangle_{\text{ph1}}^{\text{GKP}} + \beta|-\rangle_e|1\rangle_{\text{ph1}}^{\text{GKP}})|\psi\rangle_{\text{ph2}}^{\text{GKP}}. \end{aligned} \quad (\text{D3})$$

Then the electron will interact with the second photonic mode with coupling constant $g_{Q2} = \frac{a_x}{4}$. The final state will be the following:

$$\begin{aligned} |\psi_{f,3}\rangle &= S^{(2)}\left(\frac{a_x}{4}\right)|\psi_{f,2}\rangle \\ &= D^{(1)}\left(\frac{a_z}{4}\right)\left[\alpha|+\rangle_e|0\rangle_{\text{ph1}}^{\text{GKP}}D^{(2)}\left(\frac{a_x}{4}\right) \right. \\ &\quad \left. + \beta|-\rangle_e|1\rangle_{\text{ph1}}^{\text{GKP}}D^{(2)}\left(-\frac{a_x}{4}\right)\right]|\psi\rangle_{\text{ph2}}^{\text{GKP}}. \end{aligned} \quad (\text{D4})$$

Afterward, a comb electron $|+\rangle_e$ will interact with the second photonic state, creating a deterministic displacement

on the second photonic state. The coupling constant it chosen to be $g_{Q3} = -\frac{a_x}{4}$:

$$\begin{aligned} |\psi_{f,4}\rangle &= D^{(2)}\left(-\frac{a_x}{4}\right)|\psi_{f,3}\rangle \\ &= D^{(1)}\left(\frac{a_z}{4}\right)\left[\alpha|+\rangle_e|0\rangle_{\text{ph1}}^{\text{GKP}} \right. \\ &\quad \left. + \beta|-\rangle_e|1\rangle_{\text{ph1}}^{\text{GKP}}D^{(2)}\left(-\frac{a_x}{2}\right)\right]|\psi\rangle_{\text{ph2}}^{\text{GKP}}. \end{aligned} \quad (\text{D5})$$

For a GKP state $D(-\frac{a_x}{2}) = \sigma_x$. Therefore, the final state is

$$\begin{aligned} |\psi_{f,4}\rangle &= D^{(1)}\left(\frac{a_z}{4}\right)(\alpha|+\rangle_e|0\rangle_{\text{ph1}}^{\text{GKP}} + \beta|-\rangle_e|1\rangle_{\text{ph1}}^{\text{GKP}}\sigma_x)|\psi\rangle_{\text{ph2}}^{\text{GKP}} \\ &= \frac{1}{\sqrt{2}}D^{(1)}\left(\frac{a_z}{4}\right)\left[|0\rangle_e(\alpha|0\rangle_{\text{ph1}}^{\text{GKP}} + \beta|1\rangle_{\text{ph1}}^{\text{GKP}}\sigma_x) \right. \\ &\quad \left. + |1\rangle_e(\alpha|0\rangle_{\text{ph1}}^{\text{GKP}} - \beta|1\rangle_{\text{ph1}}^{\text{GKP}}\sigma_x)\right]|\psi\rangle_{\text{ph2}}^{\text{GKP}}. \end{aligned} \quad (\text{D6})$$

The final step is the electron measurement. Measuring the state $|0\rangle_e$, i.e., detecting an even energy, will create the expected CNOT gate. If the state $|1\rangle_e$ is measured, a deterministic correction can be done, using a comb electron $|+\rangle_e$ interacting with the first photonic state, to operate with a $\sigma_z^{(1)}$ Pauli operator on the final state. The probability to postselect $|0\rangle_e$ in the last step is

$$\begin{aligned} P_1 &= \frac{1}{\sqrt{2}}\left\|(\alpha|0\rangle_{\text{ph1}}^{\text{GKP}}|\psi\rangle_{\text{ph2}}^{\text{GKP}} + \beta|1\rangle_{\text{ph1}}^{\text{GKP}}\sigma_x)|\psi\rangle_{\text{ph2}}^{\text{GKP}}\right\|^2 \\ &= \frac{1}{2}(|\alpha|^2 + |\beta|^2) = \frac{1}{2}. \end{aligned} \quad (\text{D7})$$

According to the one-qubit gates section, choosing different g_Q will induce different Pauli gates on the GKP state. Choosing the coupling constant to be $g_{Q2} = -g_{Q3} = \frac{a_i}{4}$ will give a controlled Pauli $C\sigma_i$ gate.

2. Multipartite entanglement between photonic modes

In this section we show how to create an entangled state between multiple GKP states in two different ways. Using the fact that the free electron is a flying qubit, one free electron can interact with multiple GKP states, giving the ability to create multipartite entanglement.

a. Creating photonic modes GHZ state

To create a GHZ state between many GKP states, first a Hadamard gate is applied to the electron, and then a $\text{CNOT}_{e\rightarrow\text{ph}}$ gate between the free electron and each GKP state. As presented in Eq. (5) in the main text, the interaction between an electron and the GKP state can be translated to a $\text{CNOT}_{e\rightarrow\text{ph}}$ gate, where the free electron is the control qubit. To create a GHZ state using a free electron qubit, the following circuit can be applied:

$$(H_e \otimes I_{\text{ph}}^{\otimes n})\text{CNOT}_{e\rightarrow\text{ph}}^{(1)} \times \text{CNOT}_{e\rightarrow\text{ph}}^{(2)} \text{CNOT}_{e\rightarrow\text{ph}}^{(3)} \dots \text{CNOT}_{e\rightarrow\text{ph}}^{(n)} = \left[I_e \otimes D^{(1)}\left(-\frac{a_x}{4}\right)\right]S^{(1)}(g_Q)\left[I_e \otimes D^{(2)}\left(-\frac{a_x}{4}\right)\right]S^{(2)}(g_Q) \quad (\text{D8})$$

Then after applying this circuit, we will get the following state:

$$|\psi\rangle_{\text{GHZ}} = \frac{1}{\sqrt{2}}(|0\rangle_e |00\dots 0\rangle_{\text{ph}}^{\text{GKP}} + |1\rangle_e |11\dots 1\rangle_{\text{ph}}^{\text{GKP}}). \quad (\text{D9})$$

Measurement of the free-electron qubit in the X basis can then disentangle the free electron from the GKP states. After the measurement, if the measurement outcome is $|+\rangle_e$ the state will be

$$|\psi\rangle_{\text{GHZ}}^+ = \frac{1}{\sqrt{2}}(|00\dots 0\rangle_{\text{ph}}^{\text{GKP}} + |11\dots 1\rangle_{\text{ph}}^{\text{GKP}}), \quad (\text{D10})$$

and if the measurement outcome is $|-\rangle_e$ the state will be

$$|\psi\rangle_{\text{GHZ}}^- = \frac{1}{\sqrt{2}}(|00\dots 0\rangle_{\text{ph}}^{\text{GKP}} - |11\dots 1\rangle_{\text{ph}}^{\text{GKP}}). \quad (\text{D11})$$

The σ_z gate on one of the GKP states changes from the $|\psi\rangle_{\text{GHZ}}^-$ state to the $|\psi\rangle_{\text{GHZ}}^+$ state.

b. Creating photonic modes cluster states

Similarly, cluster states between a single electron and many photonic states can also be obtained. The difference between creating a cluster state and a GHZ state is the Hadamard gate between each interaction that needs to be applied to the electron, as shown in Fig. 4(a) in the main text. The following circuit is applied to create a cluster state between an electron and multiple photonic modes:

$$(H_e \otimes I_{\text{ph}}^{\otimes n}) \text{CNOT}_{e \rightarrow \text{ph}}^{(1)} (H_e \otimes I_{\text{ph}}^{\otimes n}) \text{CNOT}_{e \rightarrow \text{ph}}^{(2)} \dots (H_e \otimes I_{\text{ph}}^{\otimes n}) \text{CNOT}_{e \rightarrow \text{ph}}^{(n)} (H_e \otimes I_{\text{ph}}^{\otimes n}). \quad (\text{D12})$$

where the CNOT gate is controlled by the electron. This circuit can be written with the scattering matrix S :

$$\left[I_e \otimes D^{(1)}\left(-\frac{a_x}{4}\right) \right] S^{(1)}(g_Q) \left[H_e \otimes D^{(2)}\left(-\frac{a_x}{4}\right) \right] \times S^{(2)}(g_Q) \dots \left[H_e \otimes D^{(n)}\left(-\frac{a_x}{4}\right) \right] S^{(n)}(g_Q). \quad (\text{D13})$$

It is easier to apply a rotation gate $R_z(\frac{\pi}{2})$ on the electron since it is just an FSP. Thus, we will change the basis from X, Y, Z to the Y, Z, X basis, which means that instead of the CNOT gate, we will use the controlled Pauli σ_y , controlled by the free-electron state in the X basis. This way, the process of creating a cluster state is interaction with the photonic states with $g_Q = \frac{a_x}{4}$, with FSP between the interactions. To create cluster state in the X and Y basis, the following circuit is applied between an electron and multiple photonic modes:

$$\left[R_z\left(\frac{\pi}{2}\right) \otimes I_{\text{ph}}^{\otimes n} \right] C_x \sigma_z^{(1)} \left[R_z\left(\frac{\pi}{2}\right) \otimes I_{\text{ph}}^{\otimes n} \right] \times C_x \sigma_z^{(2)} \left[R_z\left(\frac{\pi}{2}\right) \otimes I_{\text{ph}}^{\otimes n} \right] \dots C_x \sigma_z^{(n)} \left[R_z\left(\frac{\pi}{2}\right) \otimes I_{\text{ph}}^{\otimes n} \right]. \quad (\text{D14})$$

A 2D cluster state can be created using the scheme shown in Fig. 4(b) in the main text, similarly to [71]. The photonic modes pass through the waveguide, and the distances between each interaction will constitute an FSP. After that, they go through a delay of τ and again interact; thus, it is possible

to entangle between different rows in the matrix of the 2D cluster, in a similar way as [71].

APPENDIX E: IMPROVING THE PROTOCOLS OF CREATING GKP STATES USING A SINGLE ELECTRON

The free-electron interaction can improve existing protocols for creating GKP states. Free electrons can be used in several schemes, specifically in our last paper [17] on creating GKP states using free electrons. Let us describe how to increase the probability of creating a GKP state using free electrons by utilizing feedforward, focusing on the case of creating GKP states from squeezed vacuum; in a similar way as in [14,69], the following identity holds:

$$D(i\alpha\beta)[D(\beta) - D(-\beta)]S(\xi)|0\rangle_{\text{ph}} \approx e^{i\frac{\pi}{2}} [D(\beta) + D(-\beta)]S(\xi)|0\rangle_{\text{ph}}, \quad (\text{E1})$$

where $\alpha = \frac{\pi}{4|\beta|^2}$. $S(\xi)$ is the squeezing operator with squeezing parameter ξ [90] and $|0\rangle_{\text{ph}}$ is a photonic vacuum state. The identity holds if the left displacement direction is in the same direction as the squeezing; thus $D(i\alpha\beta)S(\xi)|0\rangle_{\text{ph}} \approx S(\xi)|0\rangle_{\text{ph}}$.

For an example, we will improve on our previous work [17], on how to create a rectangular GKP state from a squeezed vacuum state. m interactions are needed with even postselection and coupling constant $g_Q = \sqrt{\pi/2}$, meaning that the final GKP state is $\propto [M^+(\sqrt{\pi/2})]^m |0\rangle_{\text{ph}}^S$. To increase the probability of success, apply correction to the state. If the electron state measured is $|1\rangle_e$, the state will evolve according to the operator $M^-(\sqrt{\pi/2})$ and it can be corrected deterministically to $M^+(\sqrt{\pi/2})$ using the identity in Eq. (E1), by interacting with another electron in the state $|+\rangle_e$ with $g_Q = i\sqrt{\pi/8}$. Specifically, there are two options for the timing of the feedforward correction. The first option is to correct the state after the first electron, meaning that if the measurement result was $|1\rangle_e$ at the first step the state will be corrected. The second option is to wait with the correction to the end, after all the electrons are measured. If all the electrons are measured in the state $|1\rangle_e$, meaning that the final state in the photonic mode is $\propto [M^-(\sqrt{\pi/2})]^m S(r)|0\rangle$, it will be corrected using a single comb electron in the state $|+\rangle_e$ with $g_Q = i\sqrt{\pi/8}$. The probability to create a GKP state with 10 dB squeezing will increase from 31.25% [17] to 62.5%.

APPENDIX F: HIGHER-ORDER DISPERSION EFFECT ON THE ELECTRON'S FIDELITY

This section considers the higher-order dispersion effects on the free-electron comb and evaluates its fidelity. We consider a comb electron with finite energy width σ in the momentum basis:

$$|+\sigma\rangle_e = \frac{1}{\sqrt{\text{Norm}}} \sum_{n=-\infty}^{\infty} e^{-\frac{n^2}{2\sigma^2}} \left| k_0 + \frac{\omega}{v} n \right\rangle. \quad (\text{F1})$$

When the electron propagates for time t , each momentum component accumulates a different phase according to the electron's dispersion relation:

$$|+\sigma^t\rangle_e = \frac{1}{\sqrt{\text{Norm}}} \sum_{n=-\infty}^{\infty} e^{-\frac{n^2}{2\sigma^2}} e^{-\frac{iE(k_0 + \frac{\omega}{v}n)t}{\hbar}} \left| k_0 + \frac{\omega}{v} n \right\rangle, \quad (\text{F2})$$

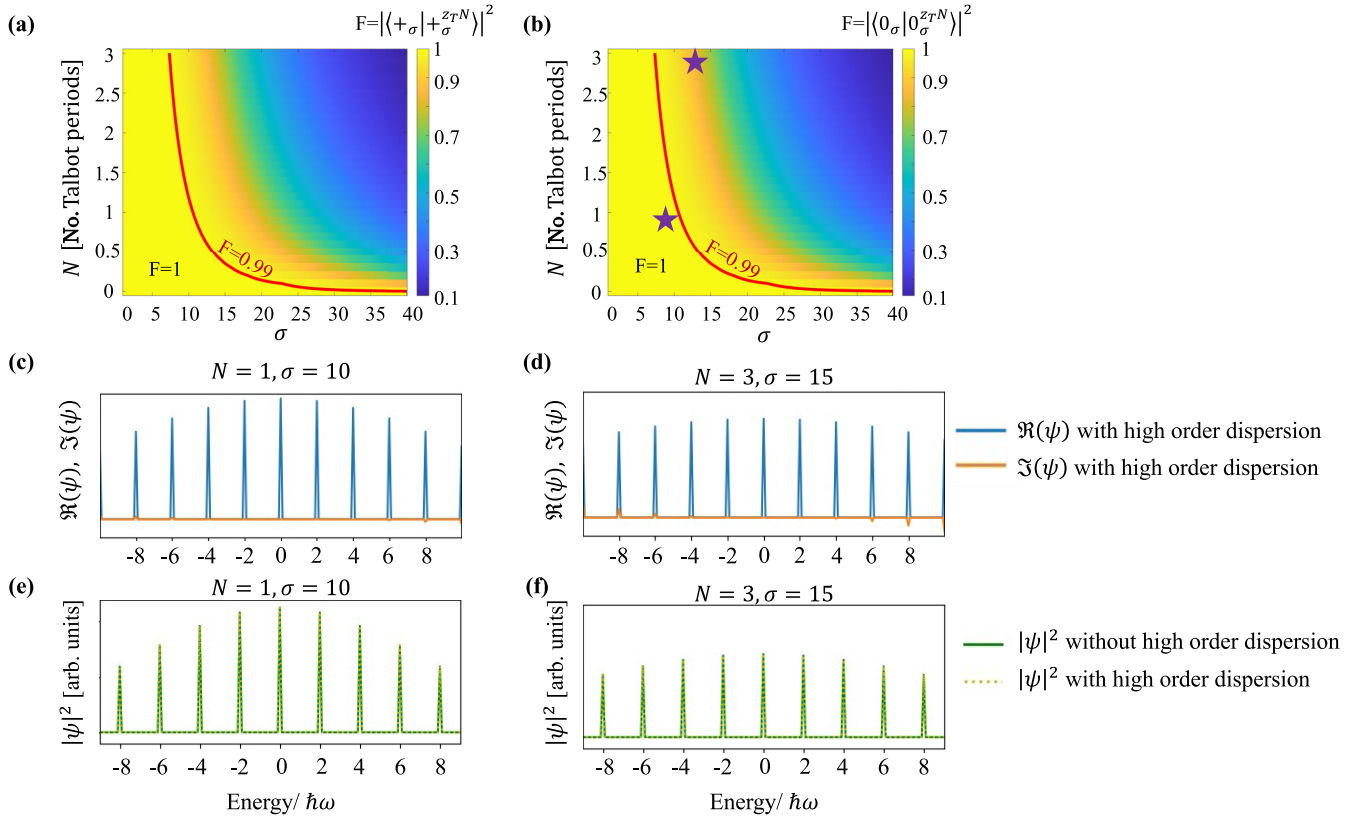


FIG. 6. Fidelity of the free-electron qubit state with high-order dispersion. (a), (b) The fidelity between the free-electron-qubit state before and after N Talbot periods, according to Eq. (F6). The fidelity is plotted as a function of the number of Talbot periods N and the electron finite energy width σ , for $|+\rangle_e$ in (a) and $|0\rangle_e$ in (b). The red curve is the 0.99 fidelity threshold; below it, the fidelity is higher than 0.99, and an extensive regime approaches a unit fidelity. (c), (d) The real and imaginary parts of the free-electron-qubit $|0\rangle_e$ wave function with high-order dispersion for different N Talbot periods and σ energy width. (e), (f) The absolute value of the free-electron-qubit $|0\rangle_e$ with and without high-order dispersion for different N Talbot periods and σ energy width. Panels (c), (e) show the wave function for $N = 1$ and $\sigma = 10$. Panels (d), (f) show the wave function for $N = 3$ and $\sigma = 15$. These points are marked with a star in (b). High-order dispersion does not change the parity of the electron and cannot rotate $|0\rangle_e$ to be $|1\rangle_e$ and vice versa.

while $E(k) = \hbar c \sqrt{k^2 + \frac{m^2 c^2}{\hbar^2}}$. It is convenient to work with the frame of reference moving with the mean electron velocity such that $t = \frac{z}{v}$ where $v = ck_0 / \sqrt{k_0^2 + \frac{m^2 c^2}{\hbar^2}}$.

We can now Taylor expand the dispersion relation of the electron around the central momentum k_0 to get

$$\begin{aligned} \frac{E(k_0 + \frac{\omega n}{v})}{\hbar} &\approx c \sqrt{k_0^2 + \frac{m^2 c^2}{\hbar^2}} + \frac{ck_0(\frac{\omega n}{v})}{\sqrt{k_0^2 + \frac{m^2 c^2}{\hbar^2}}} \\ &+ \frac{\frac{m^2 c^3}{\hbar} (\frac{\omega n}{v})^2}{2(k_0^2 + \frac{m^2 c^2}{\hbar^2})^{\frac{3}{2}}} - \frac{\frac{m^2 c^3}{\hbar} k_0 (\frac{\omega n}{v})^3}{2(k_0^2 + \frac{m^2 c^2}{\hbar^2})^{\frac{5}{2}}}. \end{aligned} \quad (\text{F3})$$

The dispersion relation can be written with v and the Talbot distance z_T [28]:

$$E\left(k_0 + \frac{\hbar\omega}{v}n\right) / \hbar \approx \frac{E_0}{\hbar} + \omega n + \frac{2\pi v}{z_T} n^2 - \frac{2\pi v \hbar\omega}{E_0 z_T} n^3. \quad (\text{F4})$$

As discussed in the main text, different operations require applying quantum gates on the electron. The universal control of the free-electron qubits (Appendix A5) requires the FSP

operation, which relies on the propagation distance of the free electron of $\frac{z_T}{4}$.

To quantify the effect of the high-order dispersion, we calculate the fidelity between the electron comb state before and after propagation of N Talbot periods. We write the state after N Talbot periods, up to an overall phase that does not change the fidelity, and up to a linear phase that only describes a shift in time and does not change the fidelity:

$$|+\sigma^{N z_T}\rangle_e = \frac{1}{\sqrt{\text{Norm}}} \sum_{n=-\infty}^{\infty} e^{-\frac{n^2}{2\sigma^2}} e^{-i2\pi n^3 N \frac{\hbar\omega}{E_0}} \left|k_0 + \frac{\omega}{v}n\right\rangle. \quad (\text{F5})$$

Note that the quadratic term in the dispersion exactly cancels out as this is the definition of the Talbot period. The resulting fidelity is

$$|\langle +\sigma | +\sigma^{N z_T} \rangle|^2 = \frac{|\sum_n e^{-\frac{n^2}{\sigma^2}} e^{-i2\pi n^3 N \frac{\hbar\omega}{E_0}}|^2}{|\sum_n e^{-\frac{n^2}{\sigma^2}}|^2}. \quad (\text{F6})$$

The third-order dispersion is proportional to the ratio between the photon energy and the electron's central energy. For typical parameters of optical frequencies and TEM electrons, the ratio $\frac{\hbar\omega}{E_0}$ is on the order of 10^{-5} . This small value makes

the high-order dispersion negligible and tolerated for quantum processing purposes. The fidelities of the free-electron wave function, with and without high-order dispersion, are plotted in Fig. 6. The electron parity cannot be changed since the high-order dispersion can rotate the electron only around the Z axis. For example, an even-comb electron will keep only even energies, and its measurement will remain independent of high-order dispersion.

The high-order dispersions present a trade-off that should be satisfied when determining the electron energy width σ . On the one side, the free-electron state fidelity decreases for large σ due to the third-order dispersion, while on the other side, the free-electron state fidelity increases with large σ (as seen in [17]). The consequences of the dispersion effects on the gates' fidelity are examined in the next section.

APPENDIX G: NOISE EFFECTS ON GATES' FIDELITIES

This section examines the impact of dispersion effects on the fidelities of the gates presented in the paper. Two noise sources need to be considered: the nonideal Gaussian envelope of the free-electron comb with variance σ and the high-order dispersion relevant to the free-space propagation (FSP). Both effects were analyzed separately in RM 5.1 of [17] and in Appendix F of this paper. Here we quantify their effects on gates' fidelities.

The CD gate used in our proposal for one qubit gate application and error correction occurs immediately after the electron is shaped. Therefore, the high-order dispersion that comes with free-space propagation does not affect it. Hence, the CD gate's primary error model is the free-electron comb's nonideality (the finite size of σ). This type of noise was studied extensively in the context of nonideal GKP noise [1,91] and was explicitly studied in the case of free-electron comb

in RM 5.1 of [17]. The conclusion is that if the normalized envelope variance σ exceeds 8, the conditional displacement gate fidelity will be larger than 0.99. There is no fundamental limit on the fidelity of this gate.

The FSP operation used in our proposal for rotation around the Z axis is affected by the high-order dispersion, thus setting the upper limit for the variance. As we show in Appendix F, a variance of $\sigma = 8$ limits the maximum number of Talbot periods to 2.5. Since only a single Talbot period is needed for the rotation gate, and a shorter FSP distance is needed for all other gates, it is possible to fulfill the trade-off between the lower and upper limits on the variance. One can always increase the fidelity further by more intricate schemes, as discussed below.

The two gate sequences relevant for universality that are limited by the high-order dispersion are the single-qubit rotation gate and the two-qubits CNOT gate. In the rotation gate, the unitary $U(\phi)$ applied to the electron, as discussed in Appendix C 5, uses FSP with one Talbot period. According to Appendix F, the upper limit for the variance is $\sigma \leq 10$. The CNOT gate uses one Hadamard gate with half a Talbot period, limiting the variance to $\sigma \leq 13$. The GHZ state creation consists solely of CD gates, and therefore σ has no upper limit. In all of the above, there is a parameter space satisfying all the dispersion limitations to achieve high gate fidelity.

Cluster state generation requires multiple Hadamard gates. By the above trade-off, if we take, for example, $\sigma = 8$, the maximum number of Talbot periods is 2.5. Thus each electron is limited to five Hadamard gates, creating a cluster with six modes (to achieve a fidelity greater than 0.99). This limit is not fundamental, as multiple electrons can increase the cluster size, and other schemes, such as fusion, can enlarge the cluster further. Even limiting to a single electron, dispersion mitigation techniques can increase the number of modes above 6.

-
- [1] D. Gottesman, A. Kitaev, and J. Preskill, Encoding a qubit in an oscillator, *Phys. Rev. A* **64**, 012310 (2001).
 - [2] S. L. Braunstein and P. van Loock, Quantum information with continuous variables, *Rev. Mod. Phys.* **77**, 513 (2005).
 - [3] S. Takeda and A. Furusawa, Toward large-scale fault-tolerant universal photonic quantum computing, *APL Photonics* **4**, 060902 (2019).
 - [4] N. Imoto, H. A. Haus, and Y. Yamamoto, Quantum nondemolition measurement of the photon number via the optical Kerr effect, *Phys. Rev. A* **32**, 2287 (1985).
 - [5] S. Pirandola, S. Mancini, D. Vitali, and P. Tombesi, Constructing finite-dimensional codes with optical continuous variables, *Europhys. Lett.* **68**, 323 (2004).
 - [6] D. Su, C. R. Myers, and K. K. Sabapathy, Conversion of Gaussian states to non-Gaussian states using photon-number-resolving detectors, *Phys. Rev. A* **100**, 052301 (2019).
 - [7] M. Eaton, R. Nehra, and O. Pfister, Non-Gaussian and Gottesman–Kitaev–Preskill state preparation by photon catalysis, *New J. Phys.* **21**, 113034 (2019).
 - [8] I. Tzitrin, J. E. Bourassa, N. C. Menicucci, and K. K. Sabapathy, Progress towards practical qubit computation using approximate Gottesman–Kitaev–Preskill codes, *Phys. Rev. A* **101**, 032315 (2020).
 - [9] H. M. Vasconcelos, L. Sanz, and S. Glancy, All-optical generation of states for “encoding a qubit in an oscillator, *Opt. Lett.* **35**, 3261 (2010).
 - [10] D. J. Weigand and B. M. Terhal, Generating grid states from Schrödinger-cat states without postselection, *Phys. Rev. A* **97**, 022341 (2018).
 - [11] C. Flühmann, T. L. Nguyen, M. Marinelli, V. Negnevitsky, K. Mehta, and J. Home, Encoding a qubit in a trapped-ion mechanical oscillator, *Nature (London)* **566**, 513 (2019).
 - [12] B. de Neeve, T. Long Nguyen, T. Behrle, and J. Home, Error correction of a logical grid state qubit by dissipative pumping, *Nat. Phys.* **18**, 296 (2022).
 - [13] P. Campagne-Ibarcq, A. Eickbusch, S. Touzard, E. Zalys-Geller, N. E. Frattini, V. V. Sivak, P. Reinhold, S. Puri, S. Shankar, R. J. Schoelkopf, L. Frunzio, M. Mirrahimi, and M. H. Devoret,

- Quantum error correction of a qubit encoded in grid states of an oscillator, *Nature (London)* **584**, 368 (2020).
- [14] J. Hastrup and U. L. Andersen, Protocol for generating optical Gottesman-Kitaev-Preskill states with cavity QED, *Phys. Rev. Lett.* **128**, 170503 (2022).
- [15] M. A. Nielsen and I. Chuang, *Quantum Computation and Quantum Information* (Cambridge University Press, Cambridge, 2002).
- [16] R. Raussendorf and H. J. Briegel, A one-way quantum computer, *Phys. Rev. Lett.* **86**, 5188 (2001).
- [17] R. Dahan, G. Baranes, A. Gorlach, R. Ruimy, N. Rivera, and I. Kaminer, Creation of optical cat and GKP states using shaped free electrons, *Phys. Rev. X* **13**, 031001 (2023).
- [18] V. V. Albert, J. P. Covey, and J. Preskill, Robust encoding of a qubit in a molecule, *Phys. Rev. X* **10**, 031050 (2020).
- [19] A. Eickbusch, V. Sivak, A. Z. Ding, S. S. Elder, S. R. Jha, J. Venkatraman, B. Royer, S. M. Girvin, R. J. Schoelkopf, and M. H. Devoret, Fast universal control of an oscillator with weak dispersive coupling to a qubit, *Nat. Phys.* **18**, 1464 (2022).
- [20] B. Barwick, D. J. Flannigan, and A. H. Zewail, Photon-induced near-field electron microscopy, *Nature (London)* **462**, 902 (2009).
- [21] F. J. Garcia De Abajo, A. Asenjo-Garcia, and M. Kociak, Multiphoton absorption and emission by interaction of swift electrons with evanescent light fields, *Nano Lett.* **10**, 1859 (2010).
- [22] S. T. Park, M. Lin, and A. H. Zewail, Photon-induced near-field electron microscopy (PINEM): Theoretical and experimental, *New J. Phys.* **12**, 123028 (2010).
- [23] A. Feist, K. E. Echternkamp, J. Schauss, S. V. Yalunin, S. Schäfer, C. Ropers *et al.*, Quantum coherent optical phase modulation in an ultrafast transmission electron microscope, *Nature (London)* **521**, 200 (2015).
- [24] Y. Morimoto and P. Baum, Diffraction and microscopy with attosecond electron pulse trains, *Nat. Phys.* **14**, 252 (2017).
- [25] G. M. Vanacore, I. Madan, G. Berruto, K. Wang, E. Pomarico, R. J. Lamb, D. McGrouther, I. Kaminer, B. Barwick, F. Javier García de Abajo, and F. Carbone, Attosecond coherent control of free-electron wave functions using semi-infinite light fields, *Nat. Commun.* **9**, 2694 (2018).
- [26] A. Polman, M. Kociak, and F. J. García de Abajo, Electron-beam spectroscopy for nanophotonics, *Nat. Mater.* **18**, 1158 (2019).
- [27] K. Wang, R. Dahan, M. Shentcis, Y. Kauffmann, A. B. Hayun, O. Reinhardt, S. Tsesses, and I. Kaminer, Coherent interaction between free electrons and a photonic cavity, *Nature (London)* **582**, 50 (2020).
- [28] O. Reinhardt, C. Mechel, M. Lynch, and I. Kaminer, Free-electron qubits, *Ann. Phys.* **533**, 2000254 (2021).
- [29] M. V. Tsarev, A. Ryabov, and P. Baum, Free-electron qubits and maximum-contrast attosecond pulses via temporal Talbot revivals, *Phys. Rev. Res.* **3**, 043033 (2021).
- [30] G. Braiman, O. Reinhardt, C. Mechel, O. Levi, and I. Kaminer, The synthetic Hilbert space of laser-driven free-electrons, *Quantum* **7**, 888 (2023).
- [31] O. Reinhardt and I. Kaminer, Theory of shaping electron wavepackets with light, *ACS Photonics* **7**, 2859 (2020).
- [32] S. V. Yalunin, A. Feist, and C. Ropers, Tailored high-contrast attosecond electron pulses for coherent excitation and scattering, *Phys. Rev. Res.* **3**, L032036 (2021).
- [33] K. E. Echternkamp, A. Feist, S. Schäfer, and C. Ropers, Ramsey-type phase control of free-electron beams, *Nat. Phys.* **12**, 1000 (2016).
- [34] R. Dahan, S. Nehemia, M. Shentcis, O. Reinhardt, Y. Adiv, X. Shi, O. Be'er, M. H. Lynch, Y. Kurman, K. Wang *et al.*, Resonant phase-matching between a light wave and a free-electron wavefunction, *Nat. Phys.* **16**, 1123 (2020).
- [35] J.-W. Henke, A. S. Raja, A. Feist, G. Huang, G. Arend, Y. Yang, J. Kappert, R. N. Wang, M. Möller, J. Pan, J. Liu, O. Kfir, C. Ropers, and T. J. Kippenberg, Integrated photonics enables continuous-beam electron phase modulation, *Nature (London)* **600**, 653 (2021).
- [36] A. B. Hayun, O. Reinhardt, J. Nemirovsky, A. Karnieli, N. Rivera, and I. Kaminer, Shaping quantum photonic states using free electrons, *Sci. Adv.* **7**, 4270 (2021).
- [37] R. Dahan, A. Gorlach, A. Karnieli, O. Eyal, P. Yousefi, M. Segev, A. Arie, G. Eisenstein, P. Hommelhoff, and I. Kaminer, Imprinting the quantum statistics of photons on free electrons, *Science* **373**, eabj7128 (2021).
- [38] A. Gover and A. Yariv, Free-electron-bound-electron resonant interaction, *Phys. Rev. Lett.* **124**, 064801 (2020).
- [39] R. Ruimy, A. Gorlach, C. Mechel, N. Rivera, and I. Kaminer, Toward atomic-resolution quantum measurements with coherently shaped free electrons, *Phys. Rev. Lett.* **126**, 233403 (2021).
- [40] Z. Zhao, X. Q. Sun, and S. Fan, Quantum entanglement and modulation enhancement of free-electron-bound-electron interaction, *Phys. Rev. Lett.* **126**, 233402 (2021).
- [41] B. Zhang, D. Ran, R. Ianculescu, A. Friedman, J. Scheuer, A. Yariv, and A. Gover, Quantum state interrogation using a pre-shaped free electron wavefunction, *Phys. Rev. Res.* **4**, 033071 (2022).
- [42] D. Ran, B. Zhang, R. Ianculescu, A. Friedman, J. Scheuer, A. Yariv, and A. Gover, Coherent excitation of bound electron quantum state with quantum electron wavepackets, *Front. Phys.* **10**, 547 (2022).
- [43] F. J. García de Abajo, E. J. C. Dias, and V. Di Giulio, Complete excitation of discrete quantum systems by single free electrons, *Phys. Rev. Lett.* **129**, 093401 (2022).
- [44] R. Ruimy, A. Gorlach, G. Baranes, and I. Kaminer, Superradiant electron energy loss spectroscopy, *Nano Lett.* **23**, 779 (2023).
- [45] G. Baranes, R. Ruimy, A. Gorlach, and I. Kaminer, Free electrons can induce entanglement between photons, *npj Quantum Inf.* **8**, 1 (2022).
- [46] X. Bendaña, A. Polman, and F. J. García De Abajo, Single-photon generation by electron beams, *Nano Lett.* **11**, 5099 (2011).
- [47] A. Feist, G. Huang, G. Arend, Y. Yang, J.-W. Henke, A. S. Raja, F. J. Kappert, R. N. Wang, H. Lourenço-Martins, Z. Qiu *et al.*, Cavity-mediated electron-photon pairs, *Science* **377**, 777 (2022).
- [48] N. Varkentina, Y. Auad, S. Y. Woo, A. Zobelli, J.-D. Blazit, X. Li, M. Tenc, K. Watanabe, T. Taniguchi, O. Stéphan *et al.*, Cathodoluminescence excitation spectroscopy: Nanoscale imaging of excitation pathways, *Sci. Adv.* **8**, 4947 (2022).
- [49] Y. Adiv, H. Hu, S. Tsesses, R. Dahan, K. Wang, Y. Kurman, A. Gorlach, H. Chen, X. Lin, G. Bartal, and I. Kaminer, Observation of 2D Cherenkov radiation, *Phys. Rev. X* **13**, 011002 (2023).

- [50] A. Blais, A. L. Grimsmo, S. M. Girvin, and A. Wallraff, Circuit quantum electrodynamics, *Rev. Mod. Phys.* **93**, 025005 (2021).
- [51] S. E. Nigg, H. Paik, B. Vlastakis, G. Kirchmair, S. Shankar, L. Frunzio, M. H. Devoret, R. J. Schoelkopf, and S. M. Girvin, Black-box superconducting circuit quantization, *Phys. Rev. Lett.* **108**, 240502 (2012).
- [52] D. M. Greenberger, M. A. Horne, and A. Zeilinger, Going beyond Bell's theorem, in *Bell's Theorem, Quantum Theory and Conceptions of the Universe*, edited by M. Kafatos (Springer, Dordrecht, 1989), pp. 69–72.
- [53] J. Brendel, N. Gisin, W. Tittel, and H. Zbinden, Pulsed energy-time entangled twin-photon source for quantum communication, *Phys. Rev. Lett.* **82**, 2594 (1999).
- [54] M. A. Nielsen, Optical quantum computation using cluster states, *Phys. Rev. Lett.* **93**, 040503 (2004).
- [55] S. Y. Song and C. Wang, Recent development in quantum communication, *Chin. Sci. Bull.* **57**, 4694 (2012).
- [56] O. Kfir, Entanglements of electrons and cavity photons in the strong-coupling regime, *Phys. Rev. Lett.* **123**, 103602 (2019).
- [57] V. di Giulio, M. Kociak, and F. J. G. de Abajo, Probing quantum optical excitations with fast electrons, *Optica* **6**, 1524 (2019).
- [58] G. Huang, N. J. Engelsens, O. Kfir, C. Ropers, and T. J. Kippenberg, Electron-photon quantum state heralding using photonic integrated circuits, *PRX Quantum* **4**, 020351 (2023).
- [59] F. J. García de Abajo, Optical excitations in electron microscopy, *Rev. Mod. Phys.* **82**, 209 (2010).
- [60] M. O. Scully and M. S. Zubairy, *Quantum Optics* (Cambridge University Press, Cambridge, 1999).
- [61] E. Wigner, On the quantum correction for thermodynamic equilibrium, *Phys. Rev.* **40**, 749 (1932).
- [62] B. M. Terhal, J. Conrad, and C. Vuillot, Towards scalable bosonic quantum error correction, *Quantum Sci. Technol.* **5**, 043001 (2020).
- [63] D. Gottesman and I. L. Chuang, Demonstrating the viability of universal quantum computation using teleportation and single-qubit operations, *Nature (London)* **402**, 390 (1999).
- [64] E. Knill, Quantum computing with realistically noisy devices, *Nature (London)* **434**, 39 (2005).
- [65] R. Shiloh, T. Chlouba, and P. Hommelhoff, Quantum-coherent light-electron interaction in a scanning electron microscope, *Phys. Rev. Lett.* **128**, 235301 (2022).
- [66] B. Royer, S. Singh, and S. M. Girvin, Stabilization of finite-energy Gottesman-Kitaev-Preskill states, *Phys. Rev. Lett.* **125**, 260509 (2020).
- [67] B. M. Terhal and D. Weigand, Encoding a qubit into a cavity mode in circuit QED using phase estimation, *Phys. Rev. A* **93**, 012315 (2016).
- [68] Y. Adiv, K. Wang, R. Dahan, P. Broaddus, Y. Miao, D. Black, K. Leedle, R. L. Byer, O. Solgaard, R. J. England, and I. Kaminer, Quantum nature of dielectric laser accelerators, *Phys. Rev. X* **11**, 041042 (2021).
- [69] J. E. Bourassa, R. N. Alexander, M. Vasmer, A. Patil, I. Tzitrin, T. Matsuura, D. Su, B. Q. Baragiola, S. Guha, G. Dauphinais *et al.*, Blueprint for a scalable photonic fault-tolerant quantum computer, *Quantum* **5**, 392 (2021).
- [70] N. H. Lindner and T. Rudolph, Proposal for pulsed on-demand sources of photonic cluster state strings, *Phys. Rev. Lett.* **103**, 113602 (2009).
- [71] H. Pichler, S. Choi, P. Zoller, and M. D. Lukin, Universal photonic quantum computation via time-delayed feedback, *Proc. Natl. Acad. Sci. USA* **114**, 11362 (2017).
- [72] K. S. Chou, J. Z. Blumoff, C. S. Wang, P. C. Reinhold, C. J. Axline, Y. Y. Gao, L. Frunzio, M. H. Devoret, L. Jiang, and R. J. Schoelkopf, Deterministic teleportation of a quantum gate between two logical qubits, *Nature (London)* **561**, 368 (2018).
- [73] Y. Wan, D. Kienzler, S. D. Erickson, K. H. Mayer, T. Rei Tan, J. J. Wu, H. M. Vasconcelos, S. Glancy, E. Knill, D. J. Wineland *et al.*, Quantum gate teleportation between separated qubits in a trapped-ion processor, *Science* **364**, 875 (2019).
- [74] S. Rosenblum, Y. Y. Gao, P. Reinhold, C. Wang, C. J. Axline, L. Frunzio, S. M. Girvin, L. Jiang, M. Mirrahimi, M. H. Devoret *et al.*, A CNOT gate between multiphoton qubits encoded in two cavities, *Nat. Commun.* **9**, 1 (2018).
- [75] O. L. Krivanek, T. C. Lovejoy, N. Dellby, T. Aoki, R. W. Carpenter, P. Rez, E. Soignard, J. Zhu, P. E. Batson, M. J. Lagos, R. F. Egerton, and P. A. Crozier, Vibrational spectroscopy in the electron microscope, *Nature (London)* **514**, 209 (2014).
- [76] P. Rez, T. Aoki, K. March, D. Gur, O. L. Krivanek, N. Dellby, T. C. Lovejoy, S. G. Wolf, and H. Cohen, Damage-free vibrational spectroscopy of biological materials in the electron microscope, *Nat. Commun.* **7**, 10945 (2016).
- [77] M. Boissonneault, J. M. Gambetta, and A. Blais, Dispersive regime of circuit QED: Photon-dependent qubit dephasing and relaxation rates, *Phys. Rev. A* **79**, 013819 (2009).
- [78] G. McMullan, A. R. Faruqi, D. Clare, and R. Henderson, Comparison of optimal performance at 300 keV of three direct electron detectors for use in low dose electron microscopy, *Ultramicroscopy* **147**, 156 (2014).
- [79] V. V. Sivak, A. Eickbusch, B. Royer, S. Singh, I. Tsioutsios, S. Ganjam, A. Miano, B. L. Brock, A. Z. Ding, L. Frunzio *et al.*, Real-time quantum error correction beyond break-even, *Nature (London)* **616**, 50 (2023).
- [80] A. I. Lvovsky, B. C. Sanders, and W. Tittel, Optical quantum memory, *Nat. Photonics* **3**, 706 (2009).
- [81] R. Haindl, A. Feist, T. Domröse, M. Möller, J. H. Gaida, S. V. Yalunin, and C. Ropers, Coulomb-correlated few-electron states in a transmission electron microscope beam, *Nat. Phys.* **19**, 1410 (2023).
- [82] S. Meier, J. Heimerl, and P. Hommelhoff, Few-electron correlations after ultrafast photoemission from nanometric needle tips, *Nat. Phys.* **19**, 1402 (2023).
- [83] E. Meyer-Scott, C. Silberhorn, and A. Migdall, Single-photon sources: Approaching the ideal through multiplexing, *Rev. Sci. Instrum.* **91**, 041101 (2020).
- [84] O. Kfir, H. Lourenço-Martins, G. Storeck, M. Sivis, T. R. Harvey, T. J. Kippenberg, A. Feist, and C. Ropers, Controlling free electrons with optical whispering-gallery modes, *Nature (London)* **582**, 46 (2020).
- [85] Y. Yang, C. Roques-Carmes, S. E. Kooi, H. Tang, J. Beroz, E. Mazur, I. Kaminer, J. D. Joannopoulos, and M. Soljačić, Photonic flatband resonances for free-electron radiation, *Nature (London)* **613**, 42 (2023).
- [86] K. Heijhoff, K. Akiba, R. Ballabriga, M. van Beuzekom, M. Campbell, A. P. Colijn, M. Franssen, R. Geertsema, V. Gromov, and X. Llopart Cudie, Timing performance of the Timepix4 front-end, *J. Instrum.* **17**, P07006 (2022).

- [87] M. W. Puckett, K. Liu, N. Chauhan, Q. Zhao, N. Jin, H. Cheng, J. Wu, R. O. Behunin, P. T. Rakich, K. D. Nelson, and D. J. Blumenthal, 422 Million intrinsic quality factor planar integrated all-waveguide resonator with sub-MHz linewidth, *Nat. Commun.* **12**, 934 (2021).
- [88] S. M. Barnett and D. T. Pegg, Phase in quantum optics, *J. Phys. A: Math. Gen.* **19**, 3849 (1986).
- [89] A. L. Grimsmo, J. Combes, and B. Q. Baragiola, Quantum computing with rotation-symmetric bosonic codes, *Phys. Rev. X* **10**, 011058 (2020).
- [90] C. Gerry and P. Knight, *Introductory Quantum Optics* (Cambridge University Press, Cambridge, 2004).
- [91] P. Brooks, A. Kitaev, and J. Preskill, Protected gates for superconducting qubits, *Phys. Rev. A* **87**, 052306 (2013).